MASTER OF SCIENCE IN ELECTRICAL AND ELECTRONIC ENGINEERING

Design and Analysis of a Highly Sensitive Hollow Core Photonic Crystal Fiber for Chemical Sensing

by

MAMOUDOU MAMADOU

Department of Electrical and Electronic Engineering
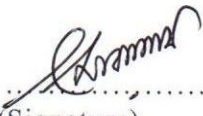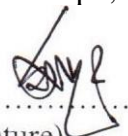
Islamic University of Technology (IUT)

The Organization of the Islamic Cooperation (OIC)

May 2019

CERTIFICATE OF APPROVAL

The thesis titled "Design and Analysis of a Highly Sensitive Hollow Core Photonic Crystal Fiber for Chemical Sensing" submitted by Mamoudou Mamadou, St. No. 161021002 of Academic Year 2018-2019 has been found satisfactory and accepted as partial fulfillment of the requirements for the Degree of Master of Science in Electrical and Electronic Engineering.

BOARD OF EXAMINERS:

1. (Signature)   Chairman
   Name: Prof. Dr. Mohammad Rakibul Islam   (Supervisor)
   Designation: Professor
   Address: EEE Dept., IUT, Gazipur-1704, Bangladesh.

2. (Signature)   Member
   Name: Prof. Dr. Md. Ruhul Amin   (Ex- Officio)
   Designation: Professor and Head
   Address: EEE Dept., IUT, Gazipur-1704, Bangladesh.

4. (Signature)(Signature)   Member

3. (Signature)   Member
   Name: Prof. Dr. Kazi Khairul Islam
   Designation: Professor
   Address: EEE Dept., IUT, Gazipur-1704, Bangladesh.
                                          Name: Prof. Dr.
                                          Md. Ashraful
                                          Hoque
   Designation: Professor
   Address: EEE Dept., IUT, Gazipur-1704, Bangladesh.

5. (Signature)   Member
   Name: Prof. Dr. Imamul Hassan Bhuiyan   (Extemal)
   Designation: Professor
   Address: EEE Dept., BUET, Dhaka

DECLARATION

It is hereby declared that this thesis or any part of it has not been submitted elsewhere for the award of any Degree.

....
(Signature of Supervisor)
Prof. Dr. Mohammad Rakibul Islam
Designation: Professor
EEE Dept., IUT, Gazipur-1704, Bangladesh.
Date: 20th March, 2019.

....
(Signature of Candidate)
Mamoudou Mamadou
Student No.: 161021002
Academic Year: 2018-2019
Date: 20th   March,   2019

TABLE OF CONTENTS

LIST OF TABLES AND FIGURES

LIST OF ABBREVIATIONS

AC:	Alternating Current
COC:	Cyclic Olefin Copolymer
COP:	Cyclic Olefin Polymer
DC:	Direct Current
DNA:	Deoxyribo-Nucleic Acid
EM:	Electromagnetic
EMI:	Electromagnetic Interference
EML:	Effective Material Loss
FDTDM:	Finite Difference Time Domain Method
FEM:	Finite Element Method
FV-FEM:	Full Vector Finite Element Method
EIM:	Effective Index Method
ISDN:	Integrated Services Digital Networks
MATLAB:	Matrix Laboratory
OF:	Fiber Optics
PBG:	Photonic Band Gap
PCF:	Photonic Crystal Fiber
PDE:	Partial Differential Equation
PML:	Perfectly Matched Layer
PMMA:	Polymethyl-Methacrylate
POF:	Plastic Optical Fiber
RI:	Refractive Index
RNA:	Ribo-Nucleic Acid
SHM:	Structural Health Monitoring
SPR:	Surface Plasmon Resonance
TV:	Television

AKNOWLEDGEMENTS

All the thanks belong first and far most to the Almighty Allah for His Bounty, Benefaction and Mercy for guiding me to the end of this tremendous effort. Afterwards, this work would never have been possible without the help and contributions of certain individuals, that is the reason why I want to address my sincere gratitude to;

- ➢ My family for their moral and financial supports.
- ➢ My supervisor for his availability, guide and relentless efforts accomplished.
- ➢ All my lecturers for the great role they played in building the foundations ideal for assimilating and implementing efficiently this work.
- ➢ All the Faculty and Staff members of the EEE department for their openness, guide and advice whenever solicited.
- ➢ My classmates and colleagues with whom I worked for the cooperation and team work.
- ➢ All my friends for their moral support during hard times.
- ➢ And to all those who by one way or the other assisted me in the completion of this humble work.

ABSTRACT

In telecommunications, the two most important developments in the last few decades are mobile communication and optical fiber transmission. Due to the exponentially growing number of internet users and the world wide web being rich in graphics and video content, more and more channel bandwidth and ultra-fast transmission speed are required to accommodate the high demands of modern technologies. As a result of this, a lot of research was carried out in these past decades on optical fibers which appeared to be a potential candidate. Proving more promising than ever, advance in fiber optic technology further led to the discovery of photonic crystal fibers abbreviated PCFs. Expanding the application of optical fiber technology beyond communication and transmission, PCFs are nowadays used in various fields such as in medicine or automotive and for several other proposes. One such application is in sensing. Due to the dire need to monitor, sense and control useful and harmful chemicals for industrial, environmental and bio-medical purposes, chemical sensing has become an eminent subject among researchers. Hence this paper focuses mainly on two designs proposed so as to meet with the aim of designing an optimum chemical sensor with sensitivities close enough to perfection. A modified kagome design with a relatively high sensitivity of 99.98%, effective material loss of as low as 0.000263 cm^{-1} and low confinement of $2.394 \times 10^{-14} \text{ cm}^{-1}$ using water, ethanol and benzene as analytes is first observed while considering other parameters such as non-linearity, dispersion, numerical aperture and effective area, which are equally investigated and discussed. In the light to reduce design complexity, a second design was proposed whereby a photonic crystal fiber made up of a spider-web like cladding and an octagonal core was investigated for sensing applications. Three widely used industrial liquids and/or by-products namely; water, acetic acid and glycerol have been investigated using Finite Element Method (FEM). Extremely high sensitivities of 99.5%, 99.7% and 99.9% were achieved at 4.5 THz for water, acetic acid and glycerol respectively. In addition to the sensitivity, parameters such as Effective Material Loss (EML), confinement loss, nonlinearity and dispersion equally showed well enhanced results compared to previous related works. The results obtained were tabulated and compared to recent works published.

APPENDIX

COMSOL MULTIPHYSICS SOFTWARE OVERVIEW

3.1. Introduction

COMSOL MULTIPHYSICS is a cross-platform finite element analysis, solver and multi-physics simulation software package. It allows conventional physics-based user interfaces and coupled systems of partial differential equations (PDEs) for various physics and engineering applications, especially coupled phenomena, or multi-physics. COMSOL contains an App Builder which can be used to develop independent domain-specific apps with custom user-interface. Users may use drag-and-drop tools (Form Editor) or programming (Method Editor). COMSOL was started in July 1986 by Svante Littmarck and Farhad Saeidi at the Royal Institute of Technology (KTH) in Stockholm, Sweden.

3.2. Running a Simulation in COMSOL MULTIPHYSICS

Generally, to run a simulation, the basic workflow is as follows;

➢ Set up model environment
➢ Create geometric objects
➢ Specify material properties
➢ Define physics boundary conditions
➢ Create mesh
➢ Run simulation Postprocess Results

3.2.1. Setting Up a Model Environment

➢ Opening the software for the first time, the user has to select the dimension he/she wants to work with. E.g. 2D, 3D or 2- and 3D axisymmetric.

➢ The required physics is then chosen based on the desired field like AC/DC, chemical, fluid flow, acoustics, plasma, heat transfer, radiofrequency, structural mechanics and mathematics. As it names indicates, COMSOL MULTIPHYSICS allows the combination or use of two or more physics at a time hence the term "Multiphysics".

➢ The type of study used for the simulation and needed in calculation is prompted for selection e.g. frequency domain. It consists of two parts;

- Pre-set studies: Consists of default studies embedded within the software e.g. Boundary Mode analysis, frequency domain, Eigen frequency, mode analysis, frequency-domain modal.

- Custom studies: This is a user-defined study such that a user can create and modified a particular study depending on his/her simulation need. Hence providing more flexibility.

➢ The last step consists of a "Units window" which shows the default unit of the model's geometrical parameters. For example, meters for length unit and degrees for angular unit are default units.

3.2.2. Geometry

Defines the geometry of the design targeted e.g. circles, ellipses, rectangles, squares, polygon. The geometries can be drawn using the COMSOL toolbox, imported from existing COMSOL file or synchronised with any other software such as Solid Works etc.

➢ Global parameters: The parameters define here are case sensitive, their units are written in square brackets and they can be used anywhere in the simulation. They are advantageous because it saves a lot of time, easily changes geometry and makes parameter sweep possible.

➢ Geometry operations: These operations are mainly of two (02) types

- Boolean operations such as union, intersection and difference.

- Transforms such as arrays, mirror, rotate, move, copy and scale

3.3.3. Defining Materials

The type and nature of material needed for simulation is chosen from this node. The COMSOL MULTIPHYSICS library is rich with a diverse variety of materials spanning different fields of engineering. Under the material node, we have;

➢ Material Library: COMSOL's in-built library listing a huge amount of material library with each material containing all of its basic properties required for a particular study already built-in or not, depending on the option taken.

➢ User defined materials: This option allows the user to define or technically create his/her desired material and define its properties.

➢ Material browser: Contains a search tab and various material libraries to facilitate research e.g. recent materials.

Materials arrangement is very important as lower nodes overrides upper nodes within the material node within the software.

3.3.4. Defining Physics Boundary Conditions

Having choose a physics, the physics boundary conditions need to be defined in order to run a simulation in COMSOL MULTIPHYSICS. Here, aspects relating to the physics based on the physics configuration and choice of study such as wave equations are added beneath the physics node by default and a configuration is expected from the user.

➢ Perfectly Matched Layer (PML): The PML boundary condition is useful when there is little or no concern regarding a model's domain e.g. a wave propagating through air. Since the air region can be infinitely long, rendering any potential

modelling tough to analyse, a PML region is added whereby the waves can propagate as if the air domain is infinitely long with little or no reflections.

➢ Scattering boundary condition: The scattering boundary condition is similar to the PML in functionality except that it is completely transparent to incoming waves which are normal to the incident boundary, reflecting some waves back as it hits the incident boundary.

3.3.5. Meshing

Defines how many spots or how many points will be calculated in the simulation. Here, the smaller the meshing the more accurate the values but the longer it takes and if the meshing is too small and too fine, the computer may run out of memory and may not be able to run anything. On the other hand, the coarser the meshing the faster the simulation and the lesser the result's accuracy. Also the finer the meshing, the heavier the COMSOL file and vice versa. Furthermore, if the mesh is well tuned, then the signal power is symmetrical otherwise it is asymmetrical.

3.3.5.1. Meshing distribution: In cases whereby a particular point is targeted to produce very good results, a meshing distribution may be used to define an independent meshing at that particular boundary. The targeted point may be the point whereby we want our EM waves to fall. Here, a desired number of elements may be defined on that boundary so as to improve the accuracy.

➢ Physics-controlled mesh: Automatically generates mesh adapting to the physics settings within the model e.g. An optic mesh differs from solid mechanic mesh or fluid mesh.

➢ User-Controlled mesh; User has menu control over the mesh size and can even create a mesh of different element types.

3.3.6. Run Simulation Post Process Results

3.3.6.1. Study

Here, the user may define the frequency at which the simulation runs and the number of modes desired. Finally, the simulation may be computed.

3.3.6.2. Analysis integrations

➢ Line integration: Help calculates signal power over given boundary or set of boundaries.

➢ Surface integration: Help calculates signal over entire surface of geometry.

3.3.6.3. Report

If a user is not too sure of a given parameter in COMSOL MULTIPHYSICS, the user can generate a complete report and see details description of each parameter with more expounded mathematical formulae under this node.

CHAPTER 1

INTRODUCTION

1.1. Background and present state of the problem:

Limitation of conventional fibers led to the invention of Photonic Crystal Fibers (PCFs). In recent years, a significant interest in the design and fabrication of photonic crystal fiber (PCF) has been undertaken due to its diverse applications and also because of its novel light guidance properties and potential for interaction of light with gases or liquids. Applicable for both communication, telecommunication and sensing applications, PCF based sensors are solicited nowadays due to their compact size, acceptable cost, design freedom and flexibility, robustness and ability to perform in hostile environments such as in high electromagnetic and high chemical exposed fields. Major PCF based sensor applications include sensing of vapors and gases, chemical sensing and medical analysis, monitoring of industrial production, marine and environmental analysis, bioprocess control, and in automotive control [1]. Furthermore, PCFs exhibit great progress in dispersion, birefringence, guiding of light in air, and nonlinear effect enhancement in the area of sensing applications that makes it unique from the conventional fibers [2]. More so, because of their diverse applications, significant research has been carried out in the design and fabrication of PCFs.

In effect, PCFs has gained massive interest in sensing applications

particularly in the terahertz domain, also known as T-ray radiation band, which occupies 0.1 to 10 THz frequency range of the electromagnetic spectrum [3]. Thus, this narrow band has been used for sensing [4], imaging [5], biotechnology [6], drug testing [7], cancer diagnosis [8], security [9], and spectroscopy [10] applications. Terahertz PCF has further become a versatile approach for applications in sensing time domain spectroscopy, biotechnology, analysis of RNA, DNA, and proteins, intraoperative breast cancer and colon cancer, diagnosis of skin cancer, and the real-time detection of cancer vs. noncancerous cells [11].

Photonic crystal fibre (PCF) uses photonic crystals to form the cladding around the core of the cable. Photonic crystal is a low-loss periodic dielectric medium constructed using a periodic array of microscopic air holes that run along the entire fibre length. *As such PCF is constructed using dielectric medium made up of microscopic air holes, which in turn, are organized in 2D array patterns.* In PCFs, photonic crystals with photonic band gaps (PBG) are constructed to prevent light propagation in certain directions with a certain range of wavelengths. Contrary to normal fibre optics, PCFs use total internal reflection or light confinement in hollow core methods to propagate light. Light propagation in PCFs is far superior to standard fibre, which uses a constant lower refractive index cladding. Photonic crystal fibre is also called micro structured- or holey fibre [12-16]. Optical fibres do not need any geometrical phenomena and thus they are based on normal operations [17-20].

PCFs are basically constructed with periodic air holes and for this reason; Refractive Index (RI) varies with change in pitch. Three different types of dielectric are generally operational: air, solid and substrate. In PCFs, varying geometrical parameters such as the pitch and air hole diameter varies the PCFs' properties [21]. Hence giving rise to numerous existing structural diversities such as circular [22], honey comb [23], spiral [24], octagonal [25], decagonal [26] and hybrid [27]. *Structural diversities vary for geometrical parameters and PCF property is determined by the diameter of holes and pitches [28].* In fact, the light guiding characteristics of PCFs are mainly determined by

- ➢ Size and spacing of the holes in the micro structure
- ➢ Refractive index of its constituent materials

Despite the availability of many and varying shapes, octagonal shapes have immense popularity in recent researches because of their geometric patterns. This type of PCF sensor is basically used in electrical field sensor, pH sensor, food processing sensor and bio-sensors. Solid core PCFs has the core with organic, metal or metal-organic material cores. Similarly, for hollow core, it consists of a void air hole and the calculation of Sellmeier equation is easier.

PCFs were initially restricted to Silica as their background material until recently whereby graphene [29], tellurite [30], PMMA (Polymethyl-methacrylate) [31], Teflon (Tetrafluoroethylene) [32] and Topas (COC) [33] are used as background materials to fabricate PCF and are reported in several works including [34, 35]. Depending on the light guiding mechanism, PCF can be categorized into two classes. One is the photonic band gap fiber (PBG-PCF), which uses the photonic band gap effect for guiding light through the fiber while Index guided fiber uses total internal reflection (TIR) to guide light through it [36]. Among the different types of PCF, hollow core is chosen for sensing applications as it allows a greater analyte volume inside its core area compared to other core types. Moreover, guided mode in a hollow core fiber has strongly confined core area, which greatly reduces the effect of the background material in wave guiding properties of the fiber [37, 38].

1.2. PCFs as Sensors

PCF sensing applications are versatile and widely used in modern days. Physical, biochemical and biological sensors are used for different features. Physical sensors may be temperature, curvature, displacement, torsion, pressure, refractive indices, electrical field, and vibration sensors. Environment, food processing, food monitoring, glucose sensors are recently added into these fields. Every form of PCF sensor has its intrinsic parameters but sensitivity differs from one another.

Biosensors implement a new aperture for diverse promising applications including biological sample tracking, antibody-antigen collaboration, medical diagnosis, organic-chemical sensing, food quality control, bio imaging, environment monitoring. For a biosensor, it generally uses the Sellmeier equation to calculate the effective refractive index, n, with respect to wavelength λ. The sensitivity of a biosensor depends on the change of wavelength and refractive indices. The ratio of peak wavelength change to refractive index is known as the sensitivity.

Evanescent sensors mostly depend on their refractive indices, relative sensitivity coefficient and effective refractive index of air holes. As the EM field varies, so the percentage also differs from one another.

Highly sensitive chemical (liquid and gas) sensors are playing a salient role in the industrial processes especially for detecting toxic and combustible chemicals (e.g. toxic gases or liquids) to overcome the safety issues. Therefore, it has become one of the key challenges, to intense the performance of liquid and gas sensors. Nowadays, researchers are keeping much concern on the development of PCF based sensors for environmental and safety monitoring issues. PCF based liquid and gas sensors through the evanescent field show peerless performance in terms of sensitivity, because PCF's core directly relates with the material to be analysed [39].

Gas sensors based on hollow-core PBGPCFs were equally proposed so as to confine more light in the core, which incorporates the gas sample. At present, most of the gas sensing techniques tend to be substantial, costly, and lack acute time data measurement; thus, surrogate sensing methods are in great demand.

In particular, SPR sensors offer many advantages such as high sensitivity as well as label-free, high sensitivity and rapid real-time detection. Because of the high sensitivity to small variations in the refractive index of the probed medium, small concentrations of bio molecules can be detected.

Temperature PCF sensors have applications in various fields such as medicine/biomedicine, the food and beverage industry, agriculture, industrial processing, and research. In the field of medicine, PCF sensors are used in real time structural health monitoring (SHM), organ transplant systems, kidney dialysis machines, and medical incubators. In the agricultural sector, they are used to monitor the temperature of plants, soil, and water. In the food and beverage industry, PCF sensors are used in fermentation, brewing, meat processing, and the manufacture of storeroom tanks. PCF temperature sensors are also versatile in the Petro-chemical industry, the automotive industry, metal industries, geo-thermal wells, electronics industry, petroleum industries, and in harsh environmental applications.

The measurement of torsion is an imperative method for the In-service evaluation and monitoring condition of engineering structures such as bridges, buildings, trains and so on.

1.3. Types of PCFs

Based on the light guiding mechanism, there are two (02) basic types of PCFs namely: Index guiding fibre and Photonic band gap fibre.

➢ Index Guiding PCF: A cladding region with air holes with diameter and pitch, running along the fibre length surrounds a solid high index core. Both core and cladding are made of same material. Nevertheless, the air holes lower the effective refractive index of the cladding creating a step index optical fibre.

➢ Photonic Bandgap Fibre: In this type of fibre, a hollow core is surrounded by a cladding region which contains air holes along the fibre length. In PBG fibre, the hollow core acts as a defect in the photonic bandgap structure, creating a region through which light can propagate.

PCFs may also be classified based on the nature of their cores as solid core, porous core or hollow core.

- ➢ Solid: Here, a solid high index solid core is having the same material with the cladding region. The cladding region equally contain air holes.

- ➢ Porous: The core, in this case, is made of different material than the cladding region. However, both regions contain air holes.

- ➢ Hollow: For this case, a hollow in made within the core of the PCF, having a different material than that of the air filled cladding region.

1.4. Unique Characteristics of PCFs

The unique characteristics of PCFs makes them advantageous over conventional fibres. They are;

- ➢ Small and compact size
- ➢ Robustness
- ➢ Acceptable cost
- ➢ Extremely low dispersion
- ➢ High birefringence
- ➢ High nonlinear effect
- ➢ Design flexibility
- ➢ Low confinement loss
- ➢ Endlessly single mode operation

1.5. Fabrication

For this research, two main designs have been proposed namely; Proposed modified kagome and spider-web respectively. With the advent of more sophisticated technologies such as the 3D printer, Sol-gel technique and the extrusion technique, the proposed sensor designs can easily be fabricated using existing fabrication techniques. A Sol-gel technique as proposed by [41, 42] can be used to fabricate PCFs with any structure while providing the possibility to adjust air-hole size, shape and spacing, resulting in a better design flexibility. *Kagome lattice PCFs with different cladding structures have been fabricated by Max Planck Institute [43]. More so, with the advent of the 3D printing technology, any types of complex preform of PCF can be printed [44, 45] and the printed preform can then extruded using the extrusion technique [46]. Kiang et al. [47] proposed an extrusion technique which allows the fabrication of almost any structure can be used to extrude the slotted air holes.* Furthermore, because a standard fiber draw may result in a ±1% variation of the total fiber diameter, sensitivity and EML curves of up to ±2% parameter variation (for the proposed modified kagome design) for a worst case scenario have been investigated and have been shown to have little or insignificant change compared to the optimum parameters. *Hence the fabrication of the proposed structure is feasible using the existing technologies.*

The most challenging aspect of manufacturing being the fiber preform, the sol-gel and 3D printing techniques are ideal candidates for design of any complex, precise or flexible structure.

1.5.1. Sol-Gel Processing Method

Interest in the sol-gel processing is dated since the mid-1800s when the hydrolysis of tetraethyl orthosilicate (TEOS) was observed to have led to the formation of SiO_2 under acidic conditions. Later on, the sol-gel grew so important that more than 35,000 papers were published worldwide on its process. [48-51]. The sol-gel process is the method used to produce solid materials from small molecules. This method is mainly used for the fabrication of metal oxides especially those of silicon (Si) and

titanium (Ti). Here, monomers are converted into a colloidal solution called sol, which acts as precursors for an integrated network called gel, of either discrete particles or network. Sol solution is a solution where particle distribution of the size of approximately 0.1-1 μm takes place in a liquid, where the only suspending force is the Brownian motion. A gel is formed when solid and liquid phases are dispersed on each other. In this process, colloidal particles are initially dispersed in a liquid forming the sol. Sol deposition then produce thin coating on any substrate by means of spraying, coating or spinning. Particles in sol are further left to polymerize by removing the stabilizing components to then produce a complex network, gel. Using appropriate coating container, precursor sol obtained can be given a desired shape. *The stages in this process have been summarized into the following [52];*

- ➤ *Mixing*: Here, the colloidal solution is formed by mechanical mixing of colloidal particles in a solvent such as water, at a precipitation preventing pH. The metal alkoxide precursor undergoes hydrolysis and poly-condensation reactions after reacting with water. A colloidal dispersion formation of extremely small particles of 1-2 nm takes place and converts into a 3-D network of the corresponding inorganic oxide.

- ➤ *Casting*: The low viscosity of the sol makes it easier for it to be casted into a mold or shape. A suitable mold choice is needed to prevent the gel from sticking to the casting container. The precursor sol can be casted into a suitable container with the desired shape e.g. to obtain monolithic ceramics, glasses or fibers. With sol viscosity adjusted into proper range, both refractory ceramics and optical fibers can be drawn which are used for thermal insulation and fiber optic sensors respectively.

- ➤ *Gelation:* The gelation process and the size of the particles decide the properties of the gel. Three dimensional networks start forming from colloidal particles and condensed silica as the gelation process takes place. In this process, there is subsequent increase in viscosity which will result in shape of casting container. With time, with controlled change in viscosity, fibers can be

spun together while gelation occurs. This results into a stock of colloidal particle as a result of interactions among the components which can be electrical in nature [53].

- *Aging: it involves the maintenance of the cast object for a period of time, ranging from hours to days. During this process, poly-condensation continues with the solution the cast object is immersed in, re-precipitating the gel network. This process decreases the porosity and increases the inter-particle neck's thickness, thus, the gel's potency is increased, producing a product resistant to cracking while drying. The aging process is also called Syneresis.*

- *Drying: Removal of remaining liquid i.e. solvent phase requires a drying process which is accompanied generally by a significant amount of densification and shrinkage. In this stage, excess solvent is removed from the complex network. A large capillary stress can develop during drying when the pores are small, causing instant cracks in the gel. These stresses can be stopped by decreasing the liquid surface. This can be achieved by eliminating very small pores, by hypercritical evaporation, which can stop the solid and liquid portions to interact. The aerogel becomes of low density after drying, gains a very good thermal insulation when placed between the glass plates and evacuated. The distribution of porosity in the gel determines the rate at which the solvent can be removed while the ultimate microstructure of the final component will be strongly influenced by changes imposed upon the structural template during this processing phase.*

- *Densification: A thermal treatment is necessary in order to further favor poly-condensation and enhance mechanical and structural stability via densification. The gel produced is densified by heating it at elevated temperatures. This further eliminate the pores in the gel, making its density approximately around fused quartz or silica. The densification temperature depends on pore dimension, surface area and pore connectivity [54]. In this*

method, densification is achieved at much lower temperatures compared to more traditional processing techniques.

This approach is a cheap and low-temperature technique that allows a fine control of the product's chemical composition. Small quantities of dopants such as organic dyes and rare-earth elements can be introduced in the sol and end up uniformly dispersed in the final product. Sol-gel derived materials equally have diverse applications in optics, electronics, energy, space, sensors, medicine such as controlled drug release and separation technology e.g. chromatography.

1.5.2. 3D Printing Method

3D printers have been around since the 1980s but were mostly used industrially and were prohibitively expensive for most, until around 2009. Today, businesses around the world are able to utilize 3D printers to produce parts for manufacturing purposes with improvements to 3D printing costs. 3D printing is also known as additive manufacturing since the numerous available 3D printing processes tend to be additive in nature with little key differences in the materials and technology used. Here, a variety of processes, equipment and materials are used to produce a three-dimensional object via additive manufacturing. This variety allows for innumerable uses by professionals, amateurs, industries or consumers alike. Additive manufacturing is where a part is made by adding material, whereas the subtractive manufacturing process is where a part is made by subtracting material. 3D printed objects can be geometrically complex and thus, are ideal in various manufacturing applications. Machines cost ranges from hundreds to millions of dollars and utilize a wide variety of technologies to print the parts. Much of this technology's growth comes from an explosion in the use of 3D printing in manufacturing, something that was previously thought impossible when the process started.

3D printed parts are being used in industries such as manufacturing, energy, and automotive. Ranging from functional prototypes, tools and fixtures to end-user

parts, the 3D printing industry is revolutionizing several other industries and processes. New materials, processes, and companies are popping up by the minute, all making promises about the unrivaled properties their parts can achieve.

The sharp drop in the cost of additive manufacturing systems between 2012 to 2018, the availability of more low-cost higher quality desktop printers widely used in industries for prototyping, fixing small custom components or additive manufacturing of actual products [55] have further made higher end 3D printers now relatively commonly used for production and additive manufacturing [56]. Many of these systems are used for prototyping before employing mass production. Almost 75% of desktop 3D printers are used in industry and not by customers [57] while military and defense are also incorporating the use of 3D printers [58, 59]. In education, higher education is another major buyer of desktop and professional 3D printers [60, 61]. Being home to research, 3D printing is used to fabricate equipment to further research and hold down costs [62]. Also, libraries around the world are locations housing smaller 3D printers for community and educational access [63].

While there are many varieties in 3D printer technologies, according to [64] there are seven most common types.

- Fused Filament Fabrication (FFF) or Fused Deposition Modeling (FDM)
- Continuous Filament Fabrication (CFF)
- Atomic Diffusion Additive Manufacturing (ADAM), also called Bound Powder Deposition
- Selective Laser Sintering/Melting (SLS/SLM)
- Direct Light Processing (DLP)
- Stereo-lithography (SLA)
- Binder Jetting

Each process and piece of equipment has advantages and disadvantages associated with it, which involve aspects such as speed, costs, geometrical limitations, tolerances, as well as appearance and mechanical properties of the products such as the texture,

color or strength. Some printers are large enough to fabricate buildings while others are micro- and Nano-scale sized objects, which generally exploits several different technologies to produce the designed product physically [65]. Both metal and glass are equally used for 3D printing but they are much more expensive and often used for works of arts.

3D printers turn computer aided design (CAD) designs into parts by building them layer by layer. For Markforged 3D printers, both metal and composite utilize processes based on Fused Filament Fabrication (FFF), the most common and affordable type of printing. In FFF, the printer heats up thermoplastic to near melting point and extrudes it out a nozzle that traces the cross section of a part for each layer, repeating this process for each layer. This is comprised of three relatively simple components [66]:

➢ 3D printing software: Relying on a fully-automated software system that controls everything from gantry position to material deposition, these systems vary significantly although they all have the same core elements.

➢ 3D printing materials: The material selection dictates both the mechanical properties of the final part and the specifics of the printing process required to fabricate it. While selecting a material, application constraints come first. However, fabrication constraints can equally make or break the part, making some materials easier to print than others.

➢ 3D printing process: This is the physical process by which FFF 3D printers deposit material layer-by-layer in the shape of a part and is dictated by software used. This process influence part quality, precision and print time.

In 3D printing, a 3D printer makes a three-dimensional object from a CAD (computer-aided design) file. Because of the variety of materials and 3D printing technologies available, it is easier more than ever to create parts for all sorts of industries. 3D printing is a relatively simple and highly automated process. [67] described 3D printing using Markforged 3D printers as follows:

- Creating a computer aided design (CAD) file: A computer aided design (CAD) file can be created by CAD software like Solidworks, Autodesk Fusion, Onshape, ANSYS, or many others.

- The file is exported from CAD as an STL file, which is the universal input file type of 3D printers.

- The exported part or STL file is then uploaded to a computer printer's slicing software. In this case, the software used for Markforged printers is called Eiger.

- Once the part is uploaded, it is oriented as desired, material and other print settings are selected and the software automatically process the part, slicing the file into layers and determining tool paths for each layer.

- After the part has been sliced, it can be printed using the print option to be printed layer-by-layer. The thickness, surface finish and durability of the finished part and materials can be controlled using different varying technologies while the print time depends on the part size.

To perform 3D printing for nanoscale-sized objects, microelectronic device fabrication methods can be employed, whereby printed objects are typically grown on a solid substrate e.g. silicon wafer, to which to adhere after printing since they are too small and fragile to be manipulated after post-construction. 3D nanostructures can equally be printed by moving a dynamic stencil mask during the material deposition process. Nanostructures with resolution as small as 10 nm have been produced using this method [68] while objects with resolution of 100 nm have been reported by [69] using an enhanced photo-polymerization process using finely-focused lasers, controlled by adjustable mirrors. Presently, 3D printing technology keeps increasing drastically. [70] reported the manufacturing of microgravity enabled optical fiber with 3D printed objects while [71] reports researchers to have that an optical fiber as thin as human hair can be used to create microscopic structures with laser based 3D printing. In a

review paper, [72] 3D nanofabrication by femtosecond laser direct writing which can be applied to micro-optics was examined with detail.

1.6. Applications of PCFs

Some applications of PCFs may include;

- ➢ Spectroscopy
- ➢ Metrology
- ➢ Biomedicine
- ➢ Imaging
- ➢ Telecommunication
- ➢ Industrial machining
- ➢ Military technology
- ➢ Sensing of chemicals, vapours and gases
- ➢ Monitoring of industrial production
- ➢ Drug monitoring
- ➢ Medical, marine and environmental analysis
- ➢ Automotive control
- ➢ Bioprocess control
- ➢ Astronomy

CHAPTER 2

LITERATURE REVIEW

2.1 Introduction

Rapid advancement in optical fiber technologies led to the discovery of Photonic Crystal Fibers (PCFs). These include high nonlinearity [75], highly negative dispersion [76], preserved single mode operation [77] just to name a few. In addition to the fact that geometrical parameters can be freely adjusted in PCFs, PCFs properties easily vary as geometrical parameters like air filling fraction (AFF), core pitch and/or air hole diameter, size or shape vary. Lately, these PCFs have been widely used in the Terahertz band as a result of their high potential to be used in various application areas of sensing and communication. However, terahertz technologies usage remains limited due to numerous practical challenges. Among them, the high losses in atmospheric conditions [78], low power generation of terahertz sources [46], difficult to integrate with other components [45] and the challenging task of designing a waveguide that transmits effectively due to high material loss of background materials. Despite these challenges, terahertz waves possess a lot of advantages and are used in far more major applications. Application areas include non-destructive security screening [80], short distance high volume wireless communication [79, 80], diagnosis of nonintrusive types of skin cancer like melanoma and basal cell carcinoma [81] and so on.

2.2. Present State Reported Works

In 1978, Yeh et al. proposed the first PCF [82]. Using a hydrothermal process, Xu et al. proposed a Zinc-Oxide (ZnO) Nano-rods for chemical analyte detection in

2006 [83] whereby the practicability of the proposed sensor was limited by the very high temperature required. In 2007 and 2008, Jepsen et al. in [84, 85] respectively proposed a method to detect chemical analytes using reflection mode terahertz time domain spectroscopy, which proved to be challenging. Terahertz time domain spectroscopy of alcohol in fuel oils was proposed by Arik et al. [86] in 2013. Ademgil proposed an octagonal PCF sensor for chemical sensing [25] in 2014, showing close to 47% sensitivity for aqueous analytes at 1.00 μm wavelength operation. Ahmed et al. [87] designed an octagonal PCF (O-PCF) with relatively high sensitivity in 2015 while sensitivity and low confinement loss was proposed in 2016 by Asaduzzaman et al. [88]. In 2016, [89] proposed a hybrid PCF with 49.17 % sensitivity. A year later, a new structure of PCF with high sensitivity, high nonlinear effect, high birefringence alongside a low confinement for chemical sensing was reported by [90]. The relative sensitivity of the design was 53.35 %. In the same year, a liquid-infiltrated PCF sensor was analyzed by [28] having a sensitivity of 55.56 %. Later on, [91] and [2] both proposed designs with relatively better sensitivities of 57.18 % and 61.45 % respectively. K. Ahmad proposed in [92] a microstructure optical fiber that can be used to sense environmental pollution, showing a relatively high sensitivity of 62.19 %. An octagonal porous cored PCF for Alcohol sensing was proposed [36], showing a relatively higher sensitivity of 67.66%. In 2018, Saiful et al. [11] proposed a highly sensitive porous core photonic crystal fiber (PC-PCF) of 85.7% at 1.6 THz, a very low dispersion and confinement loss of 0.47 ± 0.265 ps/THz/cm and 1.7×10^{-9} cm^{-1} respectively. Finally, [1] reported a sensitivity of 96.8 % using rectangular slots constituting the cladding and a square hollowed core. The design further displayed a low effective material loss, EML of 0.0035 cm^{-1} and an improved confinement loss of 6.95×10^{-14} cm^{-1}.

Previously, several research works using slotted cladding have been proposed due to many advantages resulting from using slotted designs. Slotted cladding designs such as Kagome lattice does not have band gap and thus offers very low loss in broad spectral range [93, 94], highly filled structural formation of cladding, depends on Inhibited Couplings [95] and on a mechanism similar to Von Neumann-Wigner bound conditions of the Schrödinger equation [96, 97]. Porous core PCFs are among the best

solutions for low loss efficient transmission of terahertz signal while hollow core PCFs are preferable in sensing applications as it allows a greater analyte volume within its core area and also because hollow cored fibers have strongly confined guided mode compared to porous cored fibers. This further reduces the effect of the background material in the fiber's wave guiding properties [98, 99]. In the same year Islam et al. [100] proposed a diamond core hexagonal lattice PCF whereby an EML of 0.07 cm^{-1} at 0.7 THz frequency with a large dispersion variation of 2.92 ± 0.55 ps/THz/cm.

Polymer materials are commonly used as background or bulk materials in a sensor design. A popular polymer used as bulk material is Zeonex (COP) due to its numerous useful optical properties. Zeonex has negligible water absorption, a constant refractive index of 1.53 in the terahertz frequency range, high biocompatibility, low absorption loss of 0.2 cm^{-1} and is an excellent chemical resistance even at very high temperatures [101-103] among others. Other polymers used may include Silica, Teflon (Tetrafluoroethylene), PMMA (Polymethyl-methacrylate) and Topas (COC) [102–104]. Topas and Zeonex are very similar in terms of optical characteristics though Zeonex's higher biocompatibility, higher chemical resistivity and in some cases, higher glass transitional temperature makes it suitable as a sensor and easier to fabricate [105].

Hence in this work, the main aim is to design a PCF a highly sensitive PCF with low effective material loss suitable for chemical sensing and that can be easily implemented by industries. This design should be such that its structural shape allows for a sensitivity of at least 85%, and a very EML as low as 0.003 cm^{-1}. More so, because the desired parameters to be investigated varies with PCF different geometrical shape and size, two novel designs have been proposed while considering practical feasibility of the design

CHAPTER 3

DESIGN CHOICE AND NUMERICAL ANALYSIS

3.1. *Design Choice*

Improving the performance of chemical sensors is a key challenge due to the concern for monitoring safety and environmental issues. Also, because PCF based chemical sensors show peerless performance in terms of sensitivity, a lot of research has been reported on chemical sensing. This is so because, the core of chemical sensors relates directly with the material to be sensed or analyzed. Given the multitudes of PCF designs already reported for chemical sensing, the varying refractive index, the loss in spectral range, the chemical reactivity and the core nature; An adequate design and material should be chosen such that properties aforementioned, alongside other properties like air hole size or pitch, are combined together to yield a highly performant chemical sensor.

➢ Slotted designs: They are the recent trend of PCF designs mainly because they offer low loss in a broad spectral range and relies on weak couplings between core and cladding modes.

➢ Zeonex: Zeonex has numerous desirable characteristics as discussed earlier, compared to many polymers e.g. a constant refractive index of 1.53 in THz range etc. In terms of optical characteristics, Topas and Zeonex are very similar. Nevertheless, Zeonex's higher biocompatibility, higher chemical resistivity and in some cases, higher transitional temperature makes it a better sensor than Topas; and equally easier to fabricate.

➢ Hollow cores: Hollow cored based PCF designs are unparalleled compared to porous or solid cored PCFs with respect to sensing because they have strong confined guided modes and allows a greater analyte volume within its core.

➢ Liquid sensing: Presently, compared to liquid sensing, reported works on gas sensing techniques have proven to be substantial, costly and lacking acute time data measurement.

3.2. *Numerical Analysis*

There exist several numerical methods used in EM simulations to compute the modal parameter of a given fiber in order to evaluate the overall behavior of the given PCF, such as Finite Element Method (FEM), Finite Difference Time Domain Method (FDTDM), and Effective Index Method (EIM)) are proposed for different examined microstructure PCF. Among them, the Finite element method (FEM) is the most popular. Through this method, PCF architecture is broken down from a larger complex design into smaller and simpler ones producing a better approximate solution and thus, an increased computational accuracy.

PCF with low confinement loss guarantees tight mode confinement within fiber core for a specific propagating mode. Different guiding properties of proposed PCF are numerically evaluated using Finite Element Method (FEM). The core region of the proposed PCF is filled with different commonly used industrial analytes. Overall impacts on the optical properties are investigated and an optimum result is obtained and recorded after inspection each time, alongside the optimum operating wavelength or frequency and refractive index.

3.2.1. *The Finite Element Method (FEM)*

This is a numerical technique used for solving problems described by partial differential equations or formulated as functional minimization, representing a domain of interest as an assembly of finite elements. Approximating functions in these

finite elements are determined based on the nodal values the physical field investigated and a continuous physical problem is transformed into a discretized finite element problem having unknown nodal values. Values inside finite elements can be recovered using the nodal values. For linear problems, a system of linear algebraic equations is solved. Two features of the FEM are;

➢ *Piece-wise approximation of physical fields on finite elements; ensures good precision even with simple approximating functions since in increasing the number of elements, any precision can be achieved.*

➢ *Approximation locality leads to sparse equation systems for discretized problems, thereby useful when solving problems involving large number of nodal unknowns.*

In [106], the FEM was summarized to work as follows;

➢ *Discretization: The continuum is discretized by divide a solution region into finite elements. The finite element mesh is generated by a preprocessor program and its description consists of several arrays main of nodal coordinates and element connectivity.*

➢ *Selecting Interpolation functions: Interpolation functions help to interpolate the field variables over the element and usually, polynomials are selected as interpolation functions while the number of nodes assigned to the element defines the degree of the polynomial.*

➢ *Finding the element properties: A finite element matrix equation which relates the nodal values of the unknown function to other parameters should established. This can be done using several approaches. However, the most convenient are the Galerkin method and variational approach.*

- *Assembly of element equations: This is necessary for finding the global equation system for the entire solution region i.e. combining local element equations for all elements used in discretization. Element connectivity is used for the assembly process and before solution, boundary conditions, not accounted in element equations should be imposed.*

- *Solving the global equation system: Being sparse, positive definite and symmetry in nature, direct and iterative methods can be used for solution and as a result of the solution, nodal values of the sought function are produced.*

- *Computing additional results: Quite frequently, we need to compute additional parameters e.g. strains and stresses are of interest in addition to displacements obtained after solution of the global equation system.*

Numerous approaches are used to transform finite element discrete analogue from the physical formulation of the problem (also called a differential equation). Galerkin method is the most popular finite element formulation while the variational formulation of the finite element equations are usually used for function minimization. To apply finite element procedures, a discrete model of the problem is presented in numerical form and the problem description may contain;

- *Material properties Connectivity array for finite element*
- *Scalar parameters e.g. node number or number of elements*
- *Coordinates of nodal points*
- *Arrays for description of surface and concentrated loads*
- *Coordinates of nodal points and temperature field.*

Even though finite element model can be coded by hand for simple a example, it is not the case for real-life models. Finite element models with complex shapes are created using mesh generators. This is because such models used for practical analysis can contain tens of thousands to hundreds of thousands degrees of freedom, making manual meshing impossible. Mesh generators are software tools that divides the

solution domain into many subdomains of finite elements. They can be of different types. Generally, for two-dimensional problems, block mesh generators and triangulators are used;

- ➢ *Block mesh generators: They require some initial form of gross partitioning, partitioning the solution domain in relatively small number of blocks of standard form. The mesh inside each block is generated by mapping technique.*

- ➢ *Triangulators: They generate irregular mesh inside arbitrary domains. Triangular mesh can be later transformed to the mesh consisting of quadrilateral elements. Voronoi polygons and Delaunay triangulation are widely used for mesh generation. Delaunay triangulation can also be generalized for three-dimensional domains.*

The practical applications of the FEM lead to large systems of simultaneous linear algebraic equations. Luckily, finite element equation systems possess some properties which permits to reduce storage and computing time. Finite element equation systems are symmetric, sparse and positive definite. A sparse matrix contains more zero entries than non-zero entries such that storage and computation are being economized. Symmetry allows to store just half the matrix including diagonal entries while positive definite matrices are characterized by large positive entries on the main diagonal, thus, solutions can be carried out without pivoting. Linear equation systems can be divided into two solution methods, that is, direct methods, used for moderate sized problems; and iterative methods for large problems, which in this case, are preferable because they require less computing time. Solution methods and matrix storage formats are closely related.

As with every method, FEM has some setbacks that makes it disadvantageous in some aspects. This method uses advanced mathematics which requires mathematical expertise for implementation and most importantly is the most demanding on computers.

FEM is successful in multi-physics because is a very general method which is similar to well-known and efficient structural and EM analysis methods. In addition to this, mixed formulations are equally applicable in a straight forward manner, an important factor for multi-physics analysis. By this, it combines different functions that approximates a solution within each element e.g. In EM heating, a function for heat transfer and another function for EM field is required. More so, it is easy to increase the order of elements such that the physics field approximates accurately. Again, FEM uses adaptive mesh refinement, whereby a mesh is automatically tuned (from a user perspective) to yield better result in FEM software and hence the more accurate the mesh, the better the result. Finally, curved or irregular geometries are handled naturally.

3.2.2. Equations Required

COMSOL MULTIPHYSICS version v5.3 is used here for investigating the proposed PCF. COMSOL MULTIPHYSICS is overviewed in Appendix IX. Perfectly matched layers (PML) boundary condition is applied. According to the boundary condition, PML is fixed at 10% of the entire diameter of the proposed design [95]. As given by [108, 28], the required equations are described below. An important factor in PCF designs are PCF loss properties. The EML of a PCF is given by Eq. (4.1).

$$\alpha_{eff} = \sqrt{\frac{\varepsilon_0}{\mu_0}} \left(\frac{\int_{mat} n_{mat} |E|^2 \alpha_{mat} dA}{|\int_{all} S_z dA|} \right), cm^{-1} \qquad (4.1)$$

where α_{eff} is the EML, S_z denotes the z-component of the poynting vector, μ_0 and ε_0 designate the permeability and permittivity in air respectively while α_{mat} and n_{mat} represent the bulk absorption loss and RI of Zeonex

The relative sensitivity coefficient, r, can be computed using Beer Lambert Law whereby the mutual action between light and the sensed material [109] can be understood at a particular wavelength. Sensitivity response for aqueous analytes is given by Eq. (4.2)

$$r = \frac{n_r}{Re\left[n_{\text{eff}}\right]} \times X \qquad (4.2)$$

Here, n_r is the refractive index of the sensed material, n_{eff} is modal effective index and f is the percentage of the air holes power by total power. The effective refractive index can be calculated by

$$n_{\text{eff}} = B / k_0 \qquad (4.3)$$

where B is the propagation constant, and $k_0 = 2\pi/\lambda$ is the free space wave number.

The fraction of air cavity power and the absolute power percentage represented by X can be calculated as below. Thus f can deduce as given in Eq. (4.4).

$$X = \frac{\int_{sample} Re\left(E_x H_y - E_y H_x\right) dxdy}{\int_{total} Re\left(E_x H_y - E_y H_x\right) dxdy} \times 100 \qquad (4.4)$$

where E_x and E_y are the transverse and longitudinal electric fields respectively; H_x and H_y are the transverse and longitudinal magnetic fields respectively. Effective mode area is the quantitative measurement of core area when the field mode is tightly confined within the core region. This expression is as in Eq. (4.5).

$$A_{\text{eff}} = \frac{\left(\iint |E|^2 \, dxdy\right)^2}{\iint |E|^4 \, dxdy} \qquad (4.5)$$

E indicates the electric field vector. The effective mode area of a PCF correlates with its numerical aperture (NA). This can be calculated as shown

$$NA \approx \left(1 + \frac{\pi A_{\text{eff}}}{\lambda^2}\right)^{-\frac{1}{2}} \qquad (4.6)$$

High power intensity generates lower effective mode area whereas high mode area provides lower nonlinearity. The nonlinearity (γ) of a PCF can be calculated by Eq. (4.7)

$$\gamma = \frac{n_2 \times \omega}{C \times A_{eff}} = \left(\frac{2\pi}{\lambda}\right) \times \left(\frac{n_2}{A_{eff}}\right) \left[\omega = 2\pi \, and \, C = n\lambda\right] \qquad (4.7)$$

where n_2 is the nonlinear coefficient of Zeonex; Nonlinearity (γ) is measured in $W^{-1}Km^{-1}$; C, n and λ present the velocity, frequency, and wavelength of light, respectively.

Ideally, light in PCFs should be entirely confined into the core but due to material impurities, design structure or limited number of air holes, some light are passed out of the core region leading to loss of light energy known as confinement loss. Confinement loss is a waveguide impairment causing a decrease in the signal strength of the PCF and is calculated from the imaginary part of the effective refractive index and propagation constant. It can be expressed as in Eq. (4.8).

$$L_c \left[\frac{dB}{m}\right] = \frac{20}{\ln 10} \times \frac{2\pi}{\lambda} \times Im\left(n_{eff}\right) = 8.68 k_0 \, Im\left[n_{eff}\right] \qquad (4.8)$$

where $Im\left(n_{eff}\right)$ is the imaginary part of effective refractive index, $k_0 = 2\pi\lambda$; λ is the wavelength of light.

In fiber optic transmission, dispersion can be defined as the spreading of light pulse as its travels down the length of an optical fiber, thus it is a consequence of the physical properties of the transmission medium and therefore can be reduced by the adequate fiber design choice. This can be obtained using Eq. (4.9) [110].

$$\beta_2 = \frac{2}{c} \frac{dn_{eff}}{d\omega} + \frac{\omega}{c} \frac{d^2 n_{eff}}{d\omega^2} \qquad (4.9)$$

where c is the speed of light into free space, β_2 is the dispersion parameter, $\omega = 2\pi f$ is the radian frequency and n_{eff} represents the effective refractive index.

CHAPTER 4

DESIGN I: PROPOSED MODIFIED KAGOME

4.1. Introduction

Innumerable chemical sensing reported research works have been published using water, ethanol and benzene. Benzene is a widely used industrial liquid and is also highly toxic. Ethanol in the other hand is used in food and beverage industries where it is responsible for the alcoholic nature of drinks while water is used in our daily household activities. If not properly handled, water can degrade the ecosystem and cause pollution.

As seen earlier, kagome lattice PCF offers extremely low loss in a broad spectral range [111, 93] since it does not have band gap but rather depends on a mechanism similar to Von Neumann-Wigner bound conditions of the Schrödinger equation [94, 96] and on Inhibited Coupling, which relies on weak coupling between the core and cladding modes [97]. Furthermore, the structural formation of the cladding in kagome is highly filled with air holes greatly impacting effect of the background material. The last couple of years have seen significant increase in the relative sensitivity of PCF designs. In 2017, [2] and [36] proposed sensors with sensitivities of 61.45 % and 67.66 % respectively. This was greatly improved by [11], whereby the design showed a sensitivity of 85.7 % at optimum frequencies.

Hence due to the fact that of most of these researches have failed to attain a near 100 % sensitivity mark, we propose a modified kagome hollow cored PCF with very high sensitivity and low EML in the Terahertz band for an improved sensing performance.

4.2. Design Geometry

Fig. 4.1. depicts the geometrical and parametric display of the proposed design. The proposed design consists of rectangular slots of equal lengths and widths denoted by l and w respectively, initially arranged vertically and a diameter D. The slots are then reflected 90° such that they lie horizontally on the origin and further rotated at 45° clockwise and anti-clockwise respectively to yield an array of diagonal construct on both left hand- and right hand sides of the initial vertical slot. These slots are separated by a distance Λ apart known as pitch and are fused together to form the cladding. The triangles obtained as a result of this union are defined as air holes while the rest of the cladding and PML are made up of the background material, in this case Zeonex. The perfectly matched layer (PML) is made 10% thicker than the entire diameter for an enhanced efficiency.

The core of the proposed design is made up of an octagonal shaped polygon with a core pitch, $\Lambda_c = 5$ μm and sides $P_1 = (l_1, l_2)$, $P_2 = (l_3, l_4)$, $P_3 = (l_5, l_6)$, $P_4 = (l_7, l_8)$, $P_5 = (l_9, l_{10})$, $P_6 = (l_{11}, l_{12})$, $P_7 = (l_{13}, l_{14})$, $P_8 = (l_{15}, l_{16})$ respectively as shown in Fig. 1 (b) below while Fig. 2. shows the power distribution confined within the core for both x-polarization (left) and y-polarization (right). Table 4.1. shows detailed information on the numerical value of geometrical parameters.
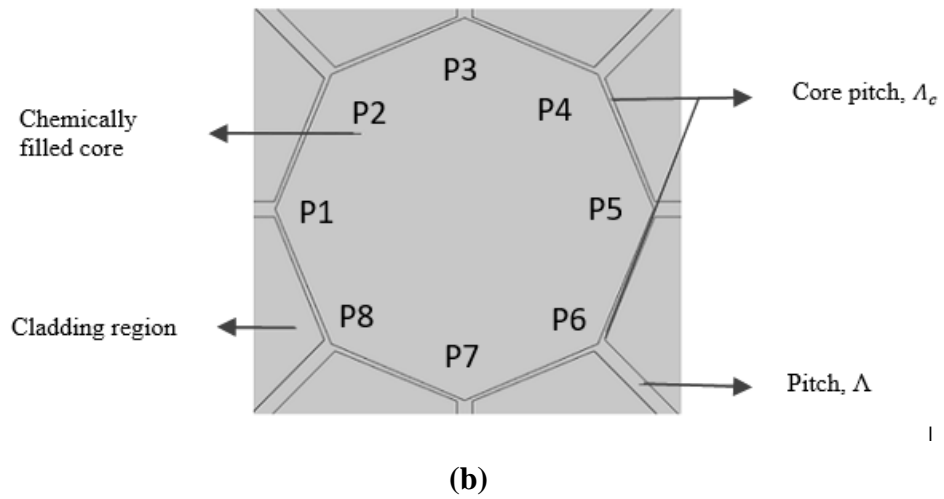

(a)

(b)
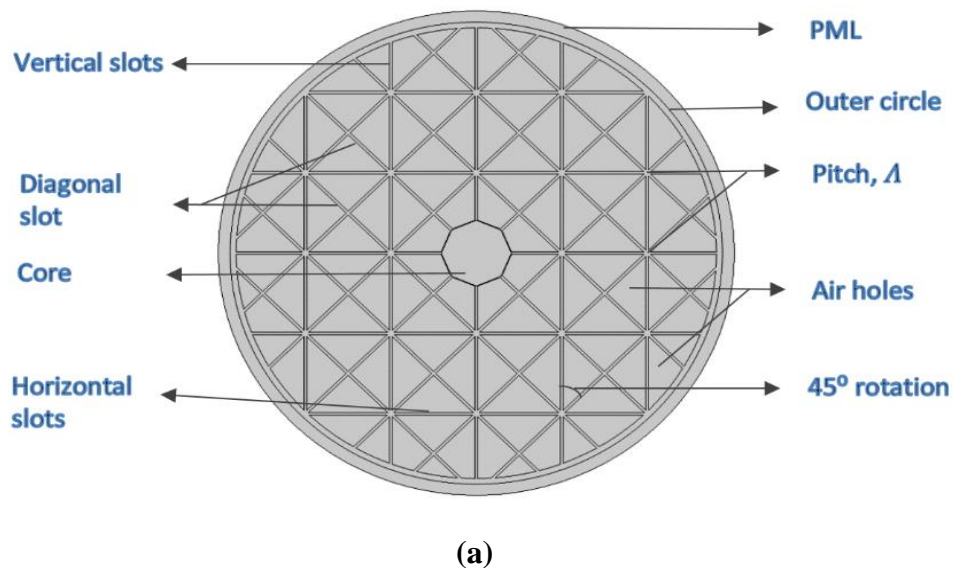
Fig. 4.1. Design geometry (a) Proposed Modified kagome (b) Octagonal Core (Magnified)
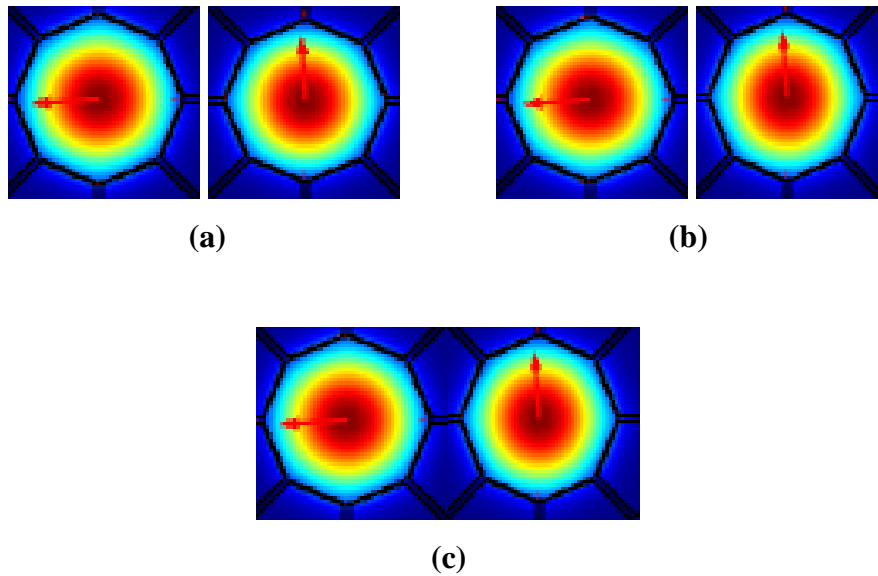

(a)

(b)

(c)

Fig. 4.2. Power distribution with x-Polarization (Left) and y-Polarization(Right) for (a) water, (b) ethanol and (c) benzene respectively

Table 4.1. Geometrical Parameters and Values

Parameter	Numerical Value	Parameter	Numerical Value
d	850 µm	l_6	245 µm
H	3200 µm	l_7	172.5 µm
l	$2 \times H$	l_8	172.5 µm
w	20 µm	l_9	245 µm
Λ	$0.93 \times d$	l_{10}	0 µm
D	$2 \times d$	l_{11}	172.5 µm
l_1	-245 µm	l_{12}	-172.5 µm
l_2	0 µm	l_{13}	0 µm
l_3	-172.5 µm	l_{14}	-245 µm
l_4	172.5 µm	l_{15}	-172.5 µm
l_5	0 µm	l_{16}	-172.5 µm

4.3. Results and Discussion

Three commonly used liquids being water, ethanol and benzene have been selected as analytes. Fig. 4.3 describes the effect on n_{eff} when varying frequency. Here, it is observed that increasing the frequency result in an increase in effective mode index.
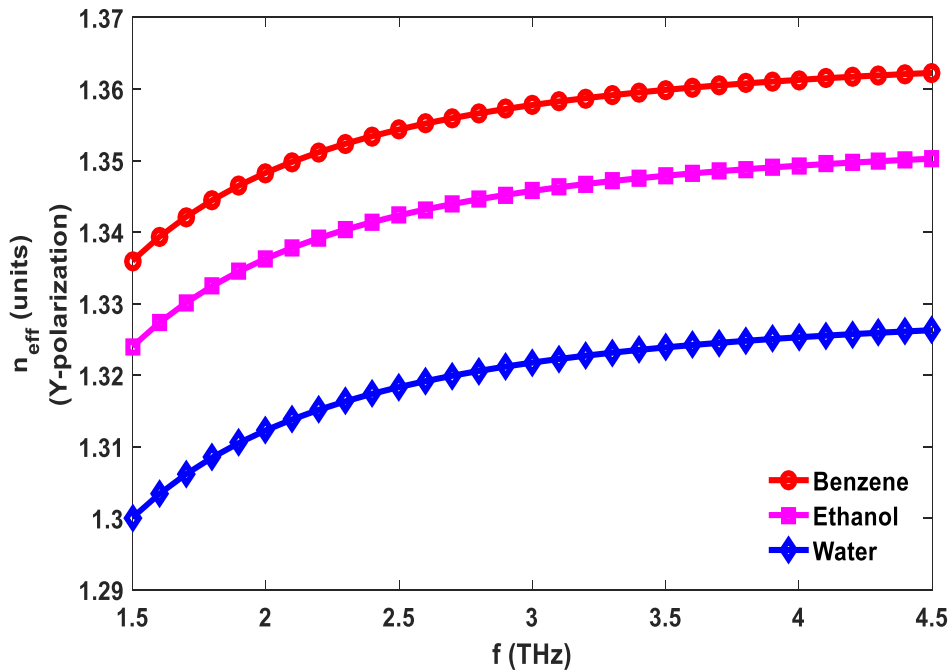
Fig. 4.3. Frequency vs. Effective Mode Index for water, ethanol and benzene

Fig. 4.4. depicts the relationship between sensitivity and frequency. It can be seen that as frequency increases, so is the sensitivity. It can further be seen that the graphs start growing exponentially up to a certain frequency and then it starts decreasing gradually as frequency increases. This is so because sensitivity is directly proportional to the core power fraction while being inversely proportional to the effective mode index as shown in Eq. (4.3) and as such at lower frequencies, both the core power fraction and effective mode indices change significantly as a result of a significant change in both the sensitivity promoting factor (core power fraction) and sensitivity degrading factor (effective mode index). At higher frequencies, however, the rate of change of core power fraction is relatively smaller than the rate of change of the effective mode indices, forcing the graph to curve downwards. This should be expected since the effective mode index increases continually with an increase in frequency whereas the core power fraction increases to a maximum value and then starts regressing with increasing frequency hence causing an overall increase and then decrease in sensitivity as the frequency moves to infinity.
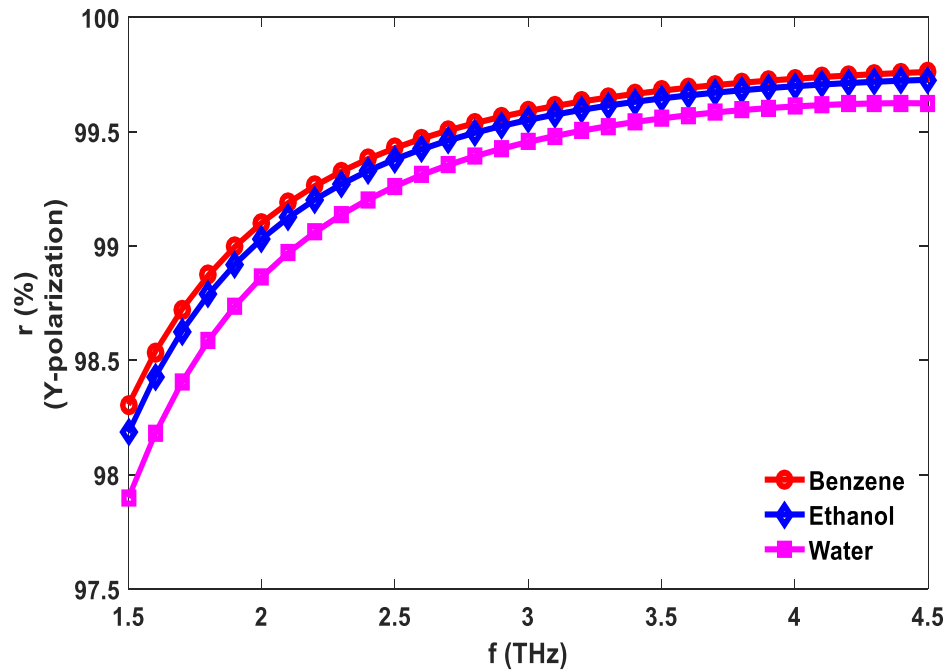
Fig. 4.4. Frequency vs. Sensitivity for water, ethanol and benzene

Fig. 4.5-4.7 shows the change in sensitivity of aqueous benzene, ethanol and water respectively when core diameter D_{core} is varied. D_{core} is chosen such that the vertices of each side of the octagon, P_1 to P_8, are equally varied so that the core's overall surface area is increased or decreased accordingly. As it can be seen, sensitivity increases as D_{core} increases and the reverse is also true i.e. sensitivity reduces with decrease in D_{core}. Increasing D_{core} implies that the core can accommodate a more significant volume of the chemical to be sensed allowing more interaction between the analyte and the fiber core thereby increasing sensitivity. Hence it can be concluded that sensitivities of the above mentioned aqueous chemical solutions are directly proportional to their D_{core}. Nevertheless, the core diameter is restricted by certain conditions preventing it to be increased infinitely. For example, for desired guiding goals, the core diameter should not overlap with the cladding. Also, for flexible fabrication of desired design, a sufficient distance should be kept between the core and cladding.
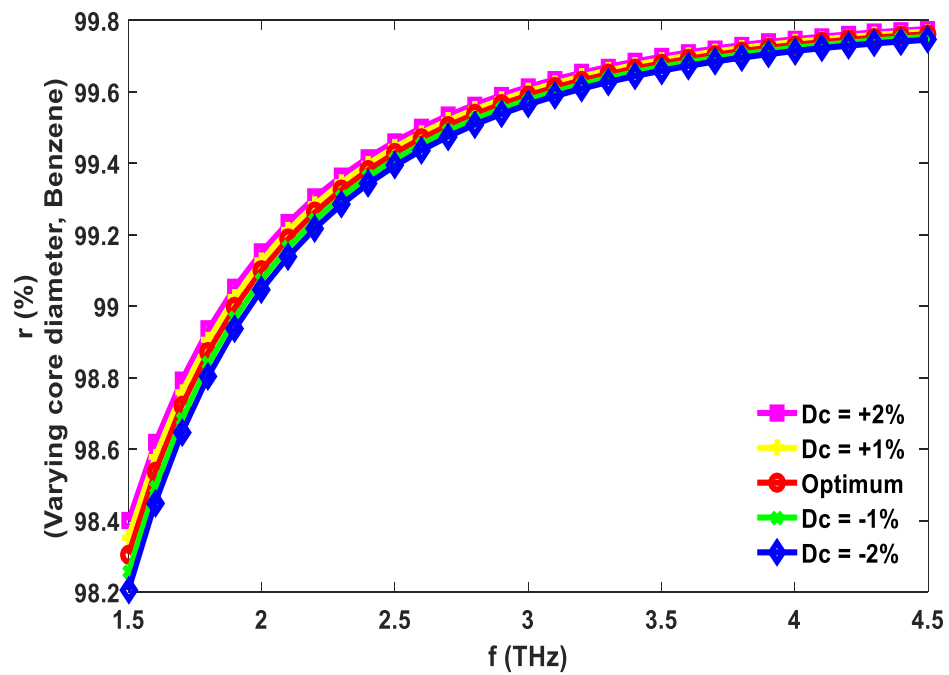
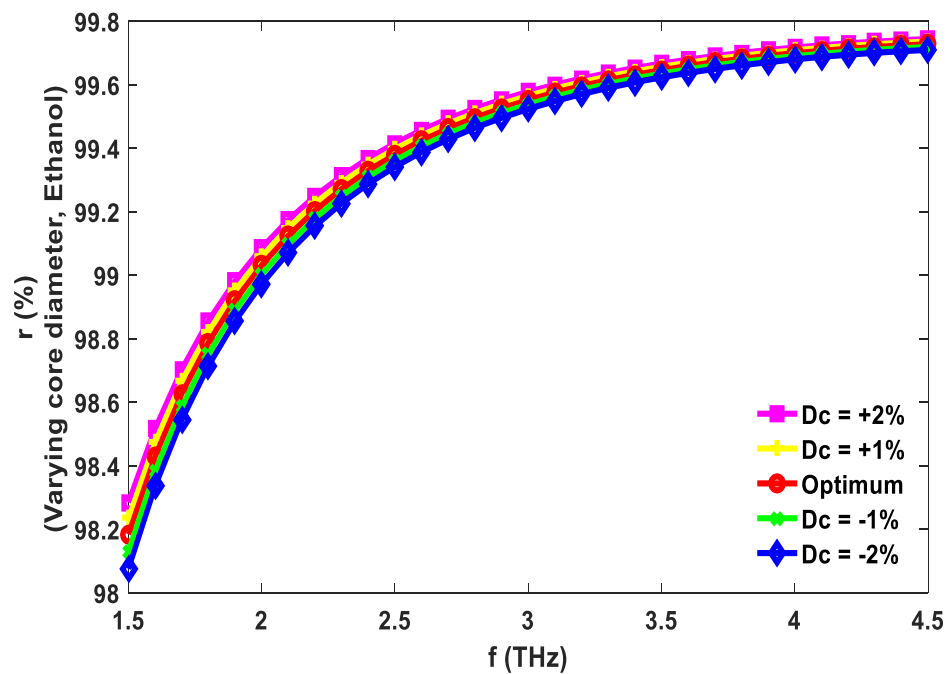**Fig. 4.5. Frequency vs Sensitivity for benzene with varying core diameter**

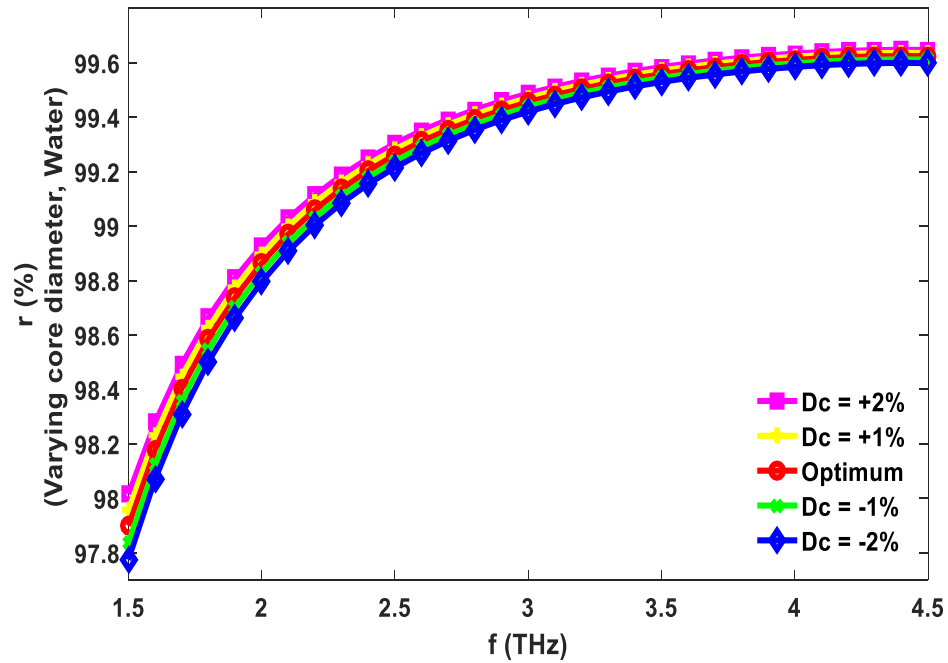**Fig. 4.6. Frequency vs Sensitivity for ethanol with varying core diameter**

Fig. 4.7. Frequency vs Sensitivity for water with varying core diameter

Fig. 4.8. relates the effect of varying frequency with respect to effective material loss (EML). EML comes in as a result of using a background material and as such depends on the surface area occupied by the background material. To reduce the effect of EML, air holes are used. More so, a hollow core further helps reduce EML by reducing the amount of space occupied by the background material. Here, it can be observed that EML reduces as frequency increases. However, at a certain frequency, EML reaches its threshold minima beyond which it starts increasing again, thereby restricting the corresponding bandwidth to a limited number of frequencies for optimal operation. This can be explained by the fact that, the more the confinement at the core, the more the overall signal power is stronger thereby overcoming the relatively weaker bulk material loss as frequency increases, resulting in a smaller bulk material to overall signal strength. At a certain frequency, core confinement becomes weaker resulting in weaker core power fraction and thus the ratio bulk material to total signal power becomes larger, hence increasing EML accordingly.
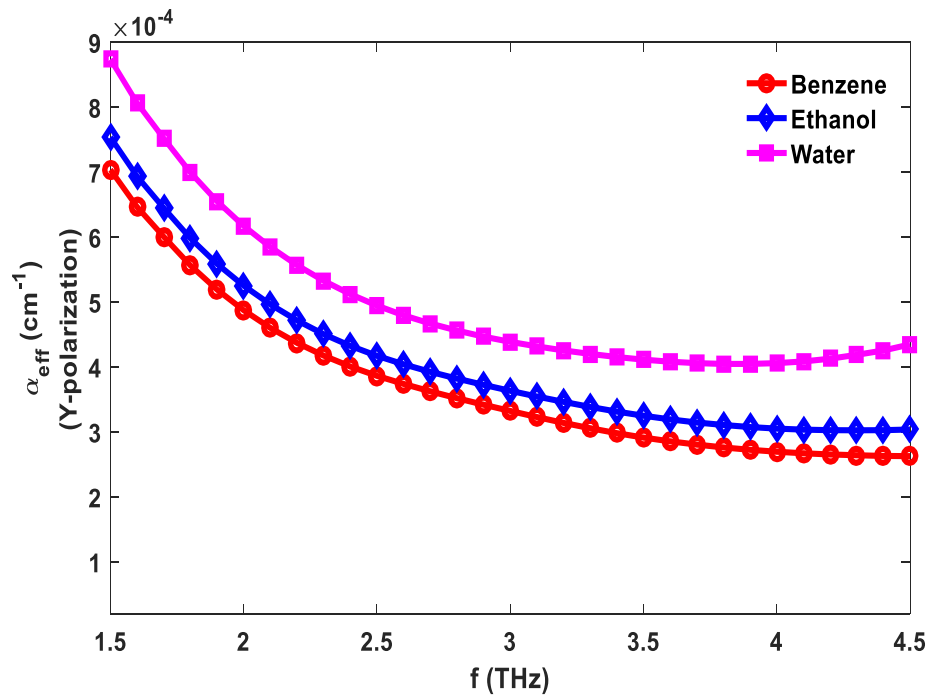
Fig. 4.8. Frequency vs. Effective Material Loss for water, ethanol and benzene

Fig. 4.9-4.11 displays the effect of varying D_{core} on EML for all three analytes. It can be seen that as diameter of core reduces, EML increases whereas core diameter increases, EML decreases. This is because as D_{core} reduces for a constant fiber diameter, D, and constant air hole size, the portion lost by D_{core} is added to the cladding region and hence to the background material thereby increasing the EML of that material. Similarly, increasing core diameter also results in a stronger signal which in turn reduces EML as explained earlier for Fig. 4.8.
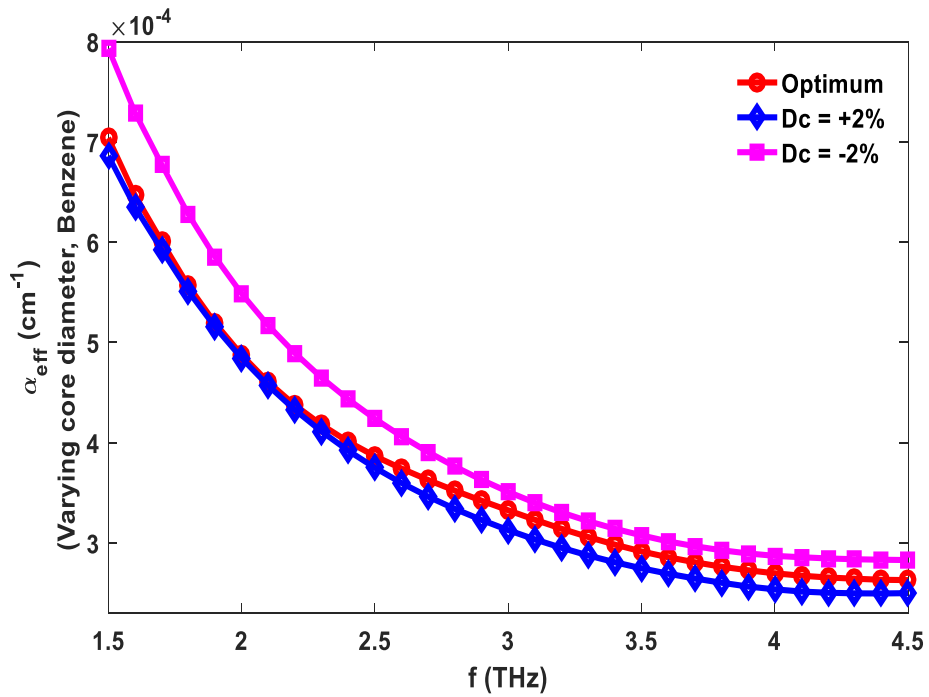
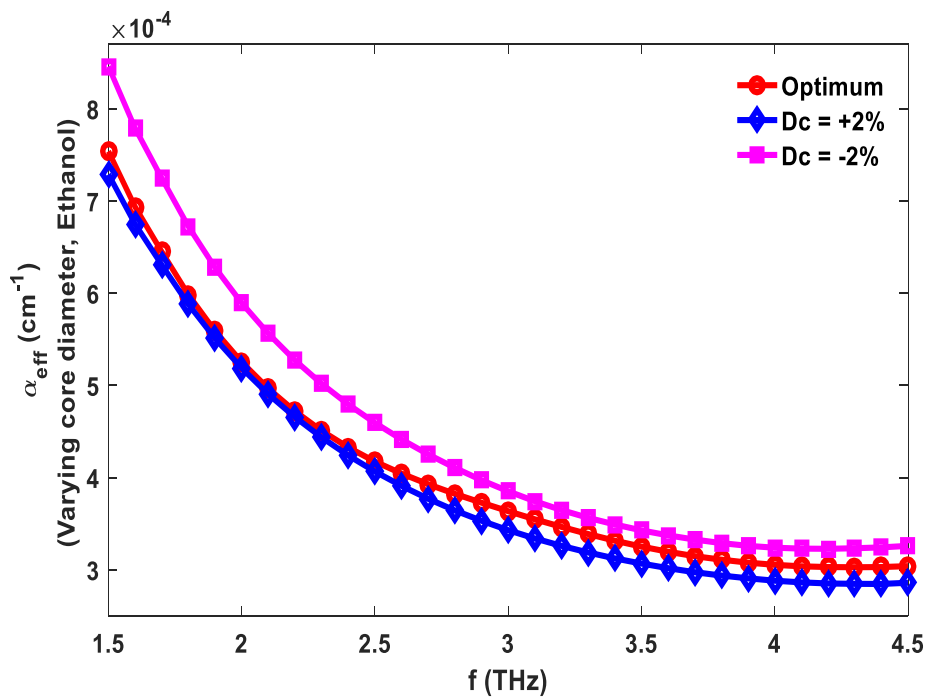**Fig. 4.9. Frequency vs EML for water with varying core diameter**

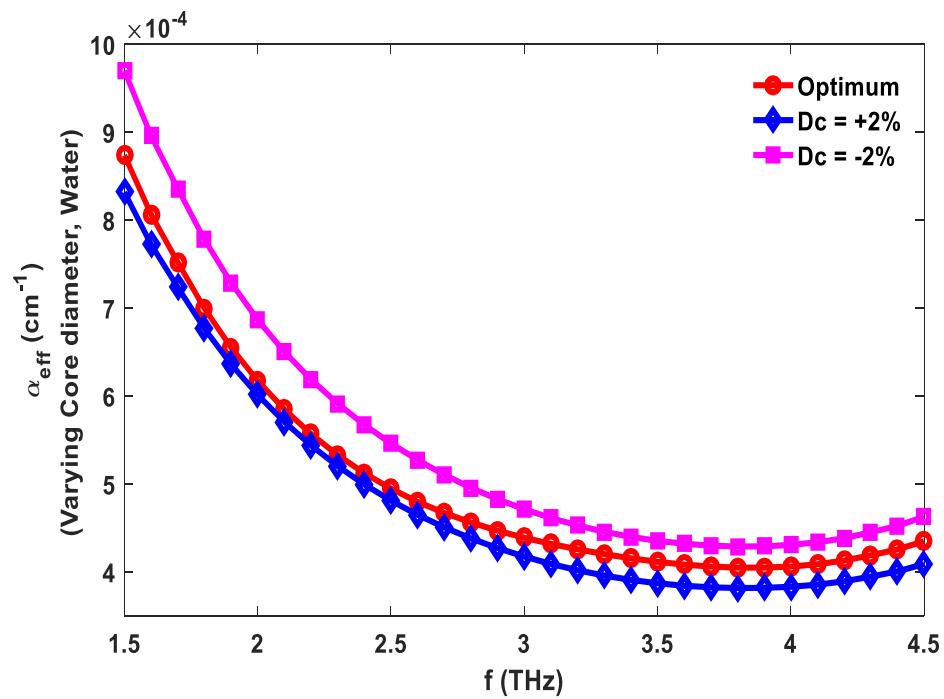**Fig. 4.10. Frequency vs EML for ethanol with varying core diameter**

Fig. 4.11. Frequency vs EML for benzene with varying core diameter

Fig. 4.12. displays information regarding the confinement loss of the three chemical analytes that are water, ethanol and benzene. It can be noted that due to the strong confinement and very high sensitivity, an extremely low confinement compared to previous published works is obtained as shown in Table 4.3.
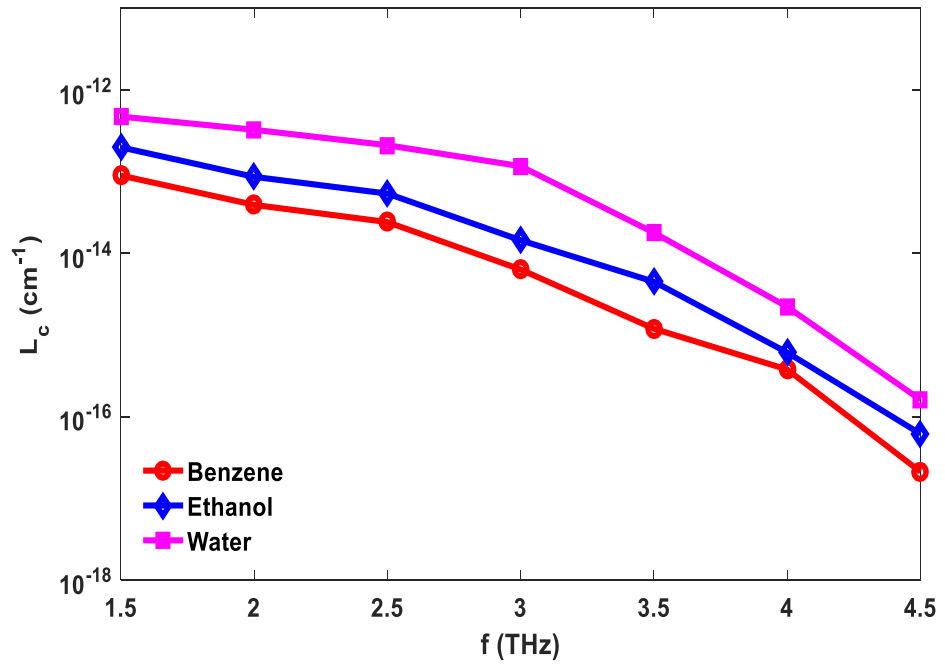
Fig. 4.12. Frequency vs. Confinement loss for water, ethanol and benzene

Fig. 4.13. depicts the change in A_{eff} with respect to frequency whereby A_{eff} reduces as frequency increases. This can be explained by the fact that as frequency increases; the signal becomes more and more confined, hence reducing the A_{eff} occupied by the signal.
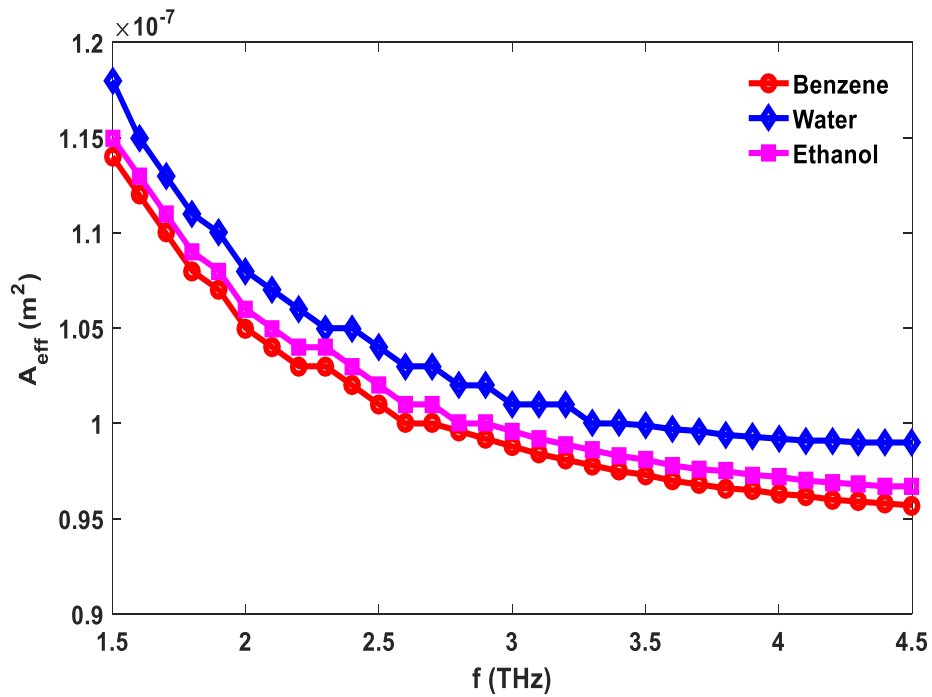
Fig. 4.13. Frequency vs. Effective Area (A_{eff}) for water, ethanol and benzene

Fig. 4.14. displays the relationship between numerical aperture (NA) and frequency. It can be seen that numerical aperture is inversely proportional to frequency provided all other parameters are kept constant. This means that as we increase the frequency, the numerical aperture is reduced accordingly. This should be expected given the fact that from its theoretical point of view, NA is inversely proportional to the effective area, which is in turn, is directly proportional to frequency.
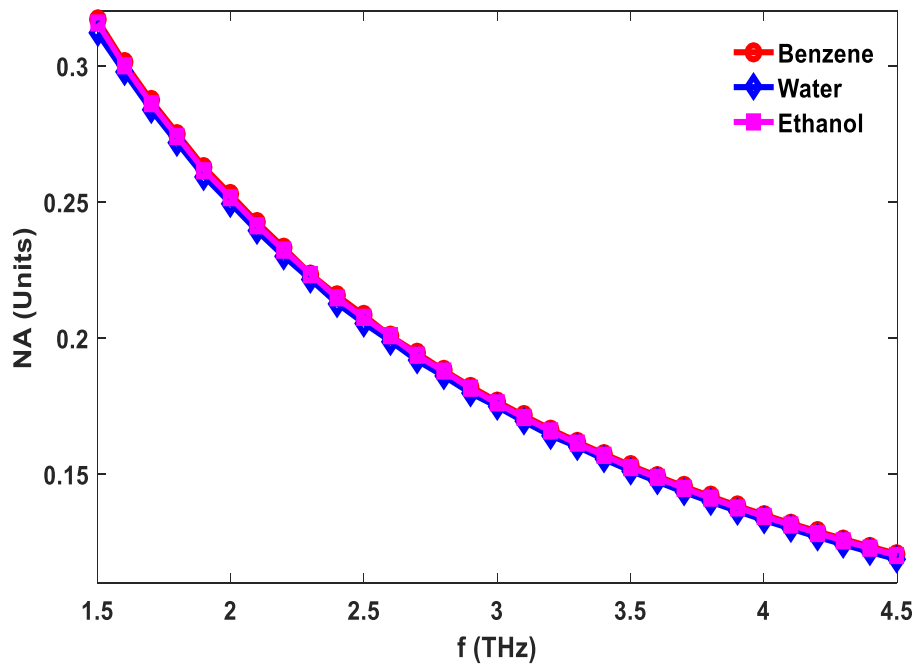
Fig. 4.14. Frequency vs. Numerical Aperture for water, ethanol and benzene

Fig. 4.15. shows the relationship between nonlinearity and frequency. It can be seen that as frequency increases, nonlinearity increases. This is due to the fact nonlinearity is inversely proportional to wavelength which in turn implies that it is directly proportional to frequency. To add to this, this behavior can be explained using the theoretical calculation of nonlinearity, whereby nonlinearity is inversely related to effective area and thus the obtained linear slope. In conclusion, analysis of both the two main varying parameters which influence the behavior of the nonlinearity vs. frequency curve which are wavelength or effective area, all results in a slope linearly increasing with frequency.
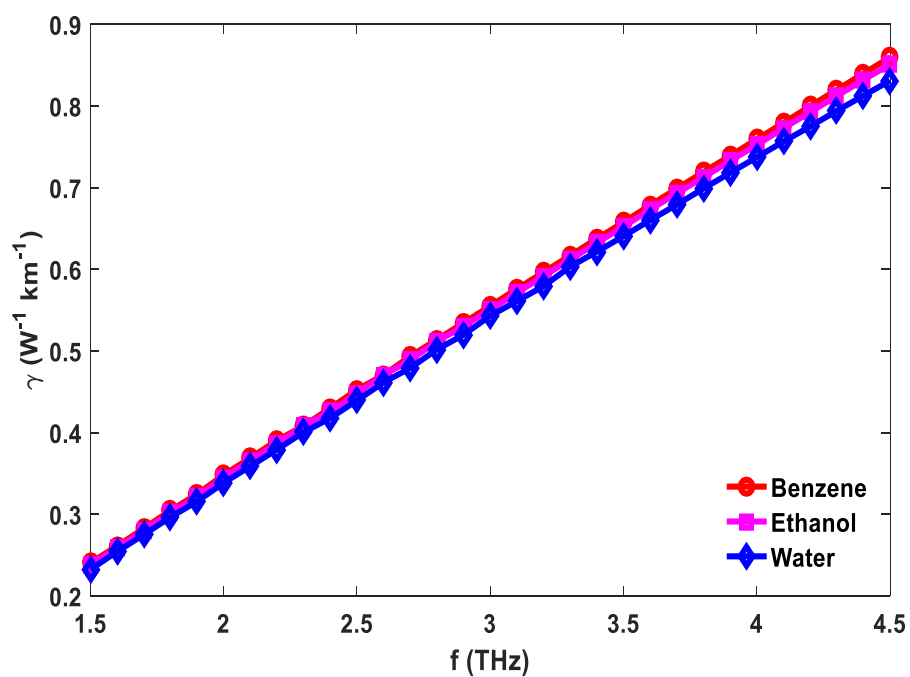
Fig. 4.15. Frequency vs. Nonlinearity for water, ethanol and benzene

Fig. 4.16. gives information about the dispersion properties of water, ethanol and benzene. Only a slight difference can be appreciated as all three analytes are closely similar in terms of dispersion.
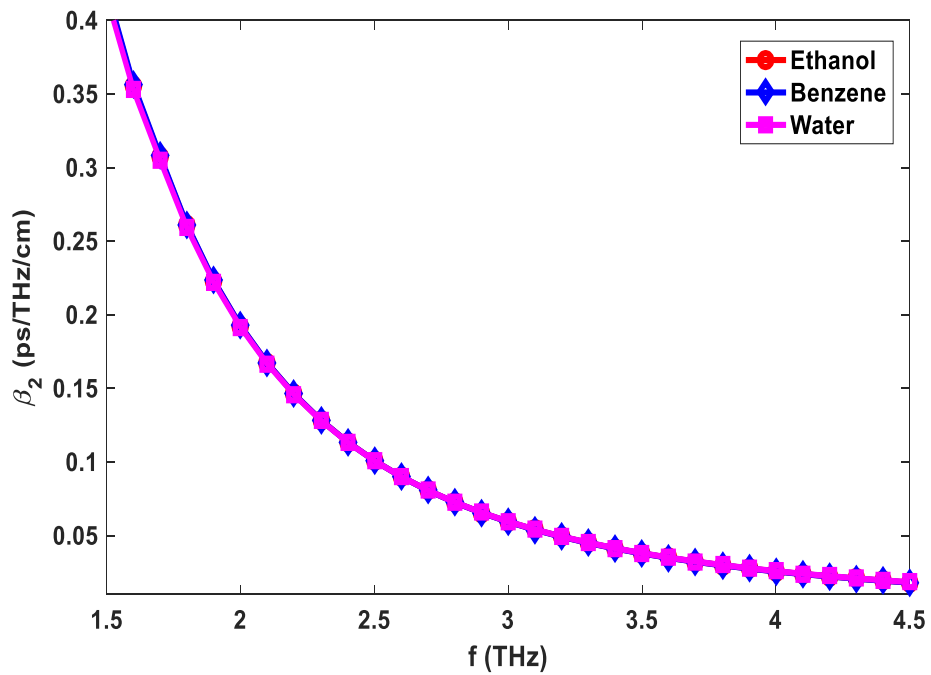
Fig. 4.16. Frequency vs. Dispersion for water, ethanol and benzene

Dispersion is an important issue for optical fiber links as it limits or restricts the information carrying capacity or bandwidth of a fiber whereby the need for dispersion compensation. Fig. 4.16 indicates that for all three chemical analytes, a dispersion less than 0.3 ps/THz/cm is obtained within the chosen frequency range which displays better results than [112].

Table 4.2. Comparison of the sensitivity and EML of the proposed modified kagome sensor design to those of previously reported sensors

PCF Designs	Sensitivity (%)	EML (cm^{-1})
[3]	-	0.052
[129]	-	$\pm$0.000416
[89]	49.17	-
[90]	53.35	-
[28]	55.56	-
[91]	57.18	-
[2]	61.45	-
[92]	62.19	-
[36]	69.09	-
[11]	85.7	-
[1]	96.8	0.0035
[45]	-	0.04
M. Kagome	99.98	0.000263

Table 4.3. Comparison of the performance characteristics between the proposed modified kagome sensor design and previously reported sensors

PCF Designs	Confinement loss (dB/m)	Dispersion (ps/THz/cm)	Numerical Aperture (units)
[3]	-	2.2$\pm$0.25	-
[129]	1.2×10^{-9}	0.4$\pm$0.042	-
[89]	6.3×10^{-11}	-	-
[90]	3.7×10^{-11}	-	-
[28]	-	-	-
[91]	1.11×10^{-11}	-	-
[2]	1.41×10^{-10}	-	0.32
[92]	5.56×10^{-11}	-	-
[36]	4.99×10^{-9}	-	-
[11]	1.7×10^{-9}	0.47 ± 0.265	0.37
[1]	6.95×10^{-14}	-	-
[45]	-	0.98 ± 0.09	-
M. Kagome	2.117×10^{-17}	0.4	0.33

4.4. Conclusion

A modified kagome with octagonal hollowed core design with a very high sensitivity of up to 99.98% and an extremely low EML of 0.000263 cm^{-1} at 4.5 THz for benzene was proposed. Key parameters such as confinement loss and dispersion among others were investigated, yielding better and highly improved results compared to previous works proposed thereby. While keeping in mind that the main challenging aspect of the proposed design is the practical feasibility of its geometrical design, an adequate fabrication method has been proposed. Finally, the proposed design is an ideal candidate as a sensor for a wide variety of sensing purposes as well as in the area of communication of the optical field.

CHAPTER 5

# DESIGN II: PROPOSED SPIDER-WEB

5.1. Introduction

Three main widely used industrial analytes that are water, glycerol and acetic acid, have been selected and analyzed for sensing purposes throughout this paper. Despite their numerous uses such as in vinegar, laxative and in daily household activities for acetic acid, glycerol and water respectively, these chemicals can equally become a hazard if not used appropriately or discarded in a safe and appropriate manner. Acetic acid for instance may damage the internal organs if ingested or if its vapor is inhaled and is highly corrosive to the skin and eyes [113], glycerol may seriously damage red blood cells during intravenous injections or may cause serious side effects in some patients when used as medication [114, 115] while water given out as an industrial by-product, if not properly discharged, may result in water pollution an important environmental concern causing diseases and degrading the ecosystem [116]. A liquid-infiltrated PCF sensor with sensitivity of 55.56 % was proposed in [28] while [91] proposed a relatively higher sensitivity of 57.18 %. In [1] reported a sensitivity of 96.8 % using rectangular slotted cladding and a square hollowed core. The design further displayed a low effective material loss, EML of 0.0035 cm^{-1} and an improved confinement loss of 6.95×10^{-14} cm^{-1} accordingly.

Therefore, a spider web-like hollow core photonic crystal fiber design is proposed in this paper. This design has a very high sensitivity nearing the 100% mark, an extremely low EML and an improved dispersion than previously reported papers.

5.2. Design Insight and Methodology

The proposed design is a spider-web like hollowed core that uses Zeonex as its bulk material. The design is made up by first constructing a pair of rectangular slots perpendicular to each other, with one lying on the vertical axes while the other lies on the horizontal axes. Another pair of rectangular slots are made to lie diagonally at an angle pi/4 to the vertical and horizontal axes as shown in Fig. 1. These horizontal, vertical and diagonal slots all have the same lengths and widths denoted by l = 2900 μm and w = 30 μm respectively. The cladding's spider-web like structure is constructed using three rectangular slots labelled R1, R2 and R3 with lengths 360 μm, 710 μm and 1070 μm respectively, all rotated at an angle of pi/8. More so, the rectangular slots R1, R2 and R3 all have equal widths, w. The core is an octagonal structure with vertices (0, 250), (177.5, 177.5), (250, 0), (177.5, -177.5), (0, -250), (-177.5, -177.5), (-250, 0) and (-177.5, 177.5) respectively, all measured in μm. The air holes within the cladding are separated by a distance Λ = 30 μm called the pitch. The octagonal core and spider-web like cladding on the other hand are separated by Λ_c = 5 μm. These design parameters are chosen such as to ensure the maximum confinement strength. The power distribution on both the X- and Y-Polarization for water, acetic acid and glycerol can be observed in Fig. 2.
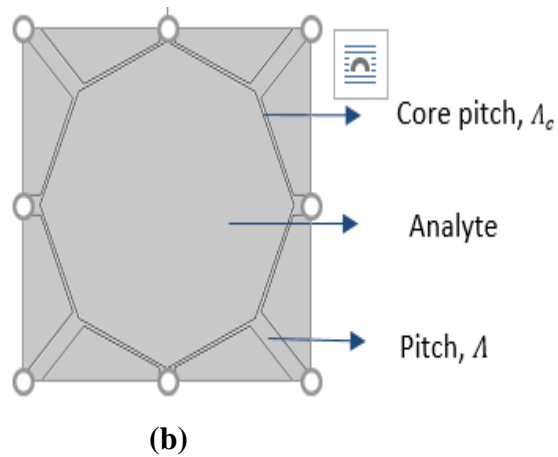

(a)

(b)
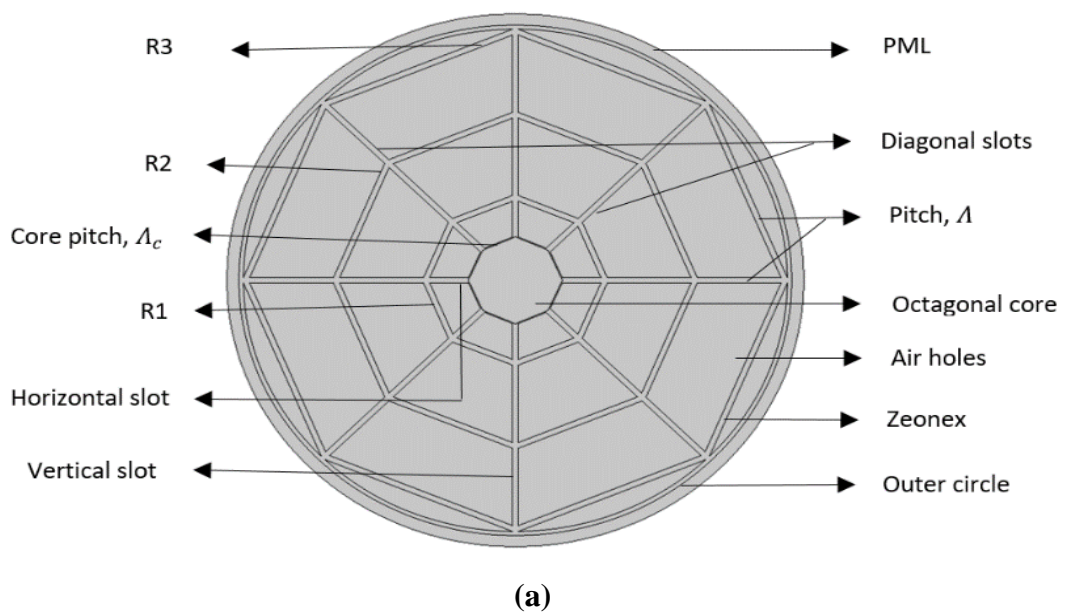
Fig. 5.1. Design geometry (a) Spider Web (b) Octagonal Core (Zoomed in)
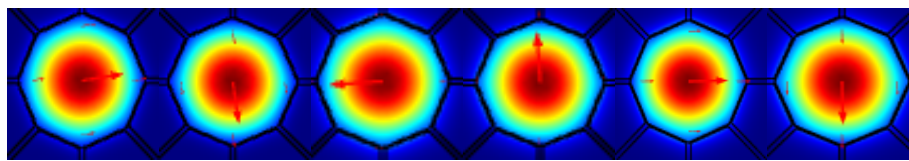

Fig. 5.2. x- and y-Polarization Power distribution from left-right for water, acetic acid and glycerol respectively

5.3. Results and Discussion

Fig. 5.3 relates the effective mode index to the operating frequencies. It can be seen that Effective index increases with frequency, with glycerol having the highest RI.

Fig. 5.4 shows the relationship between frequency and sensitivity. As frequency increases, the sensitivity also increases. The graph starts growing exponentially at first, then it starts increasing at a lower speed at the latter part of the graph. This is so because at higher frequencies, the change in the effective modal index becomes more and more negligible compared to those at lower frequencies and as a result, the sensitivity curve starts bulging downwards.
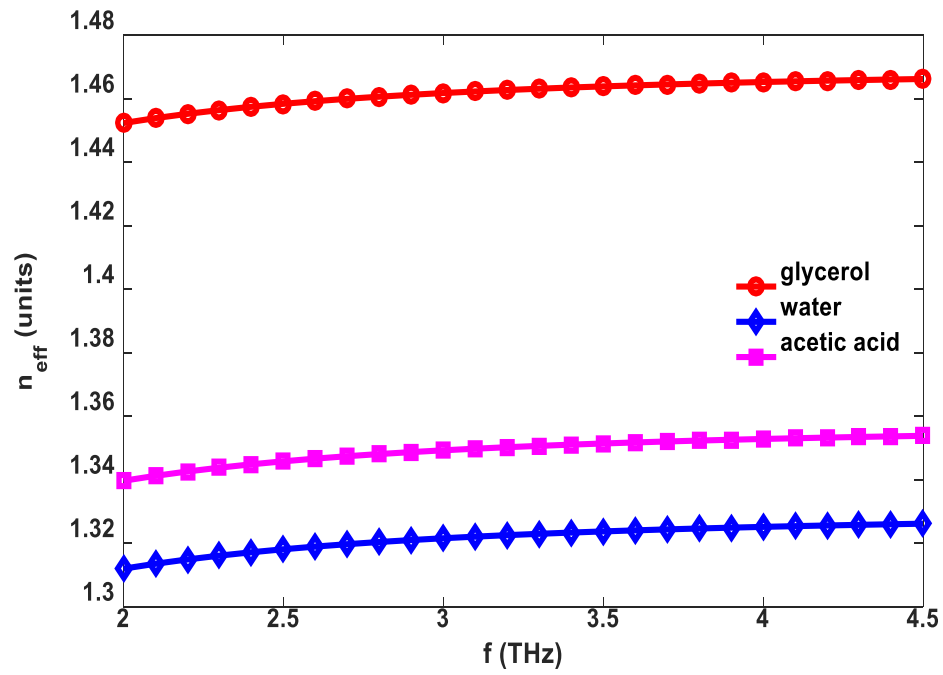
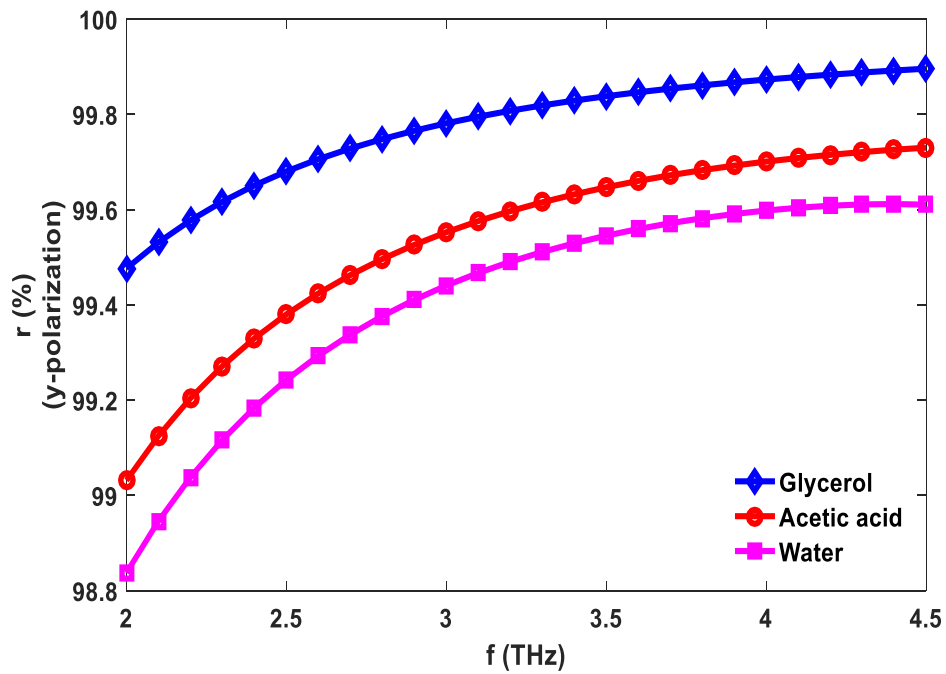**Fig. 5.3. Frequency vs. Effective Mode Index for water, acetic acid and glycerol**

Fig. 5.4. Frequency vs. Sensitivity for water, acetic acid and glycerol

Fig. 5.5 displays the effect of varying frequency with respect to effective material loss (EML). EML depends on the surface area occupied by the background material, reason why air holes are used so as to reduce the effect of EML. It can be seen that EML reduces as frequency increases. This is because the more the confinement at the core, the better and stronger the overall signal is, resulting in a smaller bulk material to overall signal strength. Nevertheless, at a certain high frequency, core confinement starts to weaken as core power fraction becomes weaker. The ratio bulk material to total signal power becomes larger and EML starts increasing again, restricting the corresponding bandwidth to a limited number of frequencies for an optimum operation.
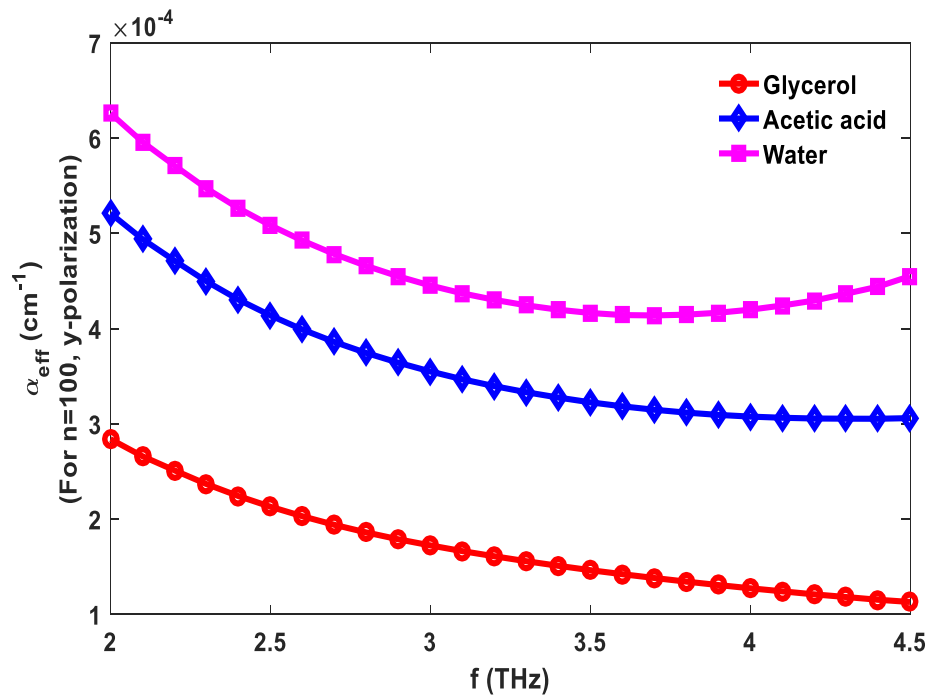
Fig. 5.5. Frequency vs. EML for water, acetic acid and glycerol

Fig. 5.6 Depicts the confinement loss with respect to water, acetic acid and glycerol. It is seen than confinement loss decreases as frequency increases. This should be expected since the confinement loss is inversely proportional to the operating frequency as given by Eq. (5.3) above.
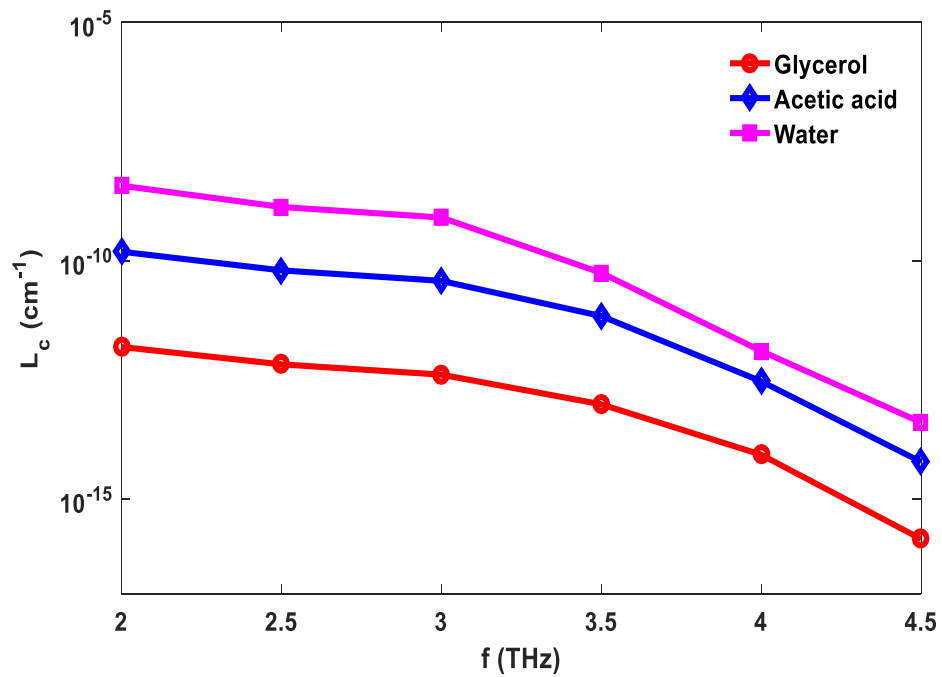
Fig. 5.6. Frequency vs. Confinement loss for water, acetic acid and glycerol

Fig. 5.7 displays the relationship between nonlinearity and frequency and it can be noted that nonlinearity increases linearly with frequency. This is so because nonlinearity is inversely proportional to wavelength, implying that it is directly proportional to frequency and hence the linear relationship.
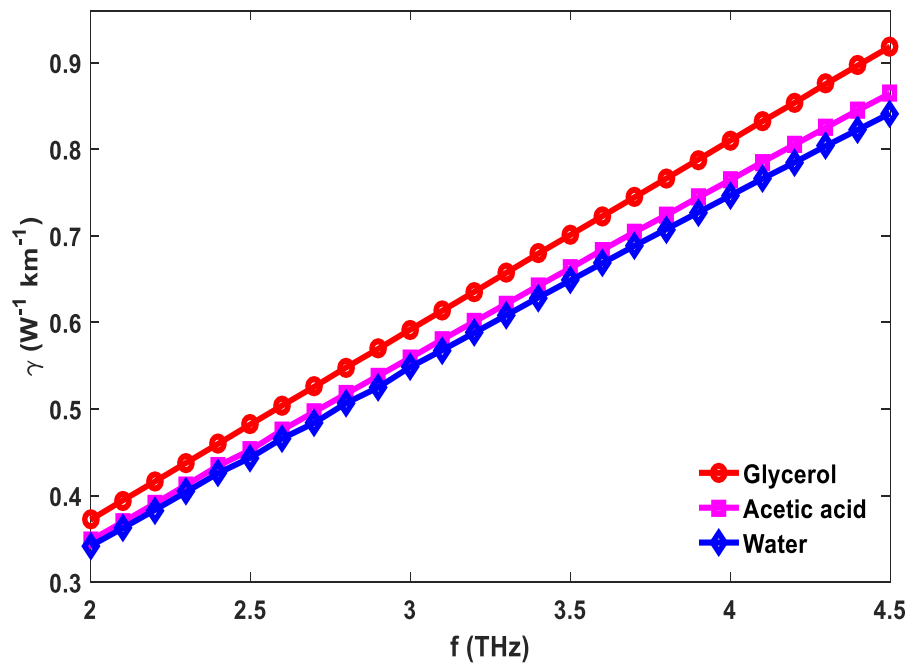
Fig. 5.7. Frequency vs. Nonlinearity for water, acetic acid and glycerol

As shown in Fig. 5.8, dispersion decreases with increase in frequency. This should be expected since dispersion depends on the rate of change of the modal effective index and as explained earlier for sensitivity, as we move towards higher frequencies, the rate of change of the modal effective index decreases and hence dispersion.
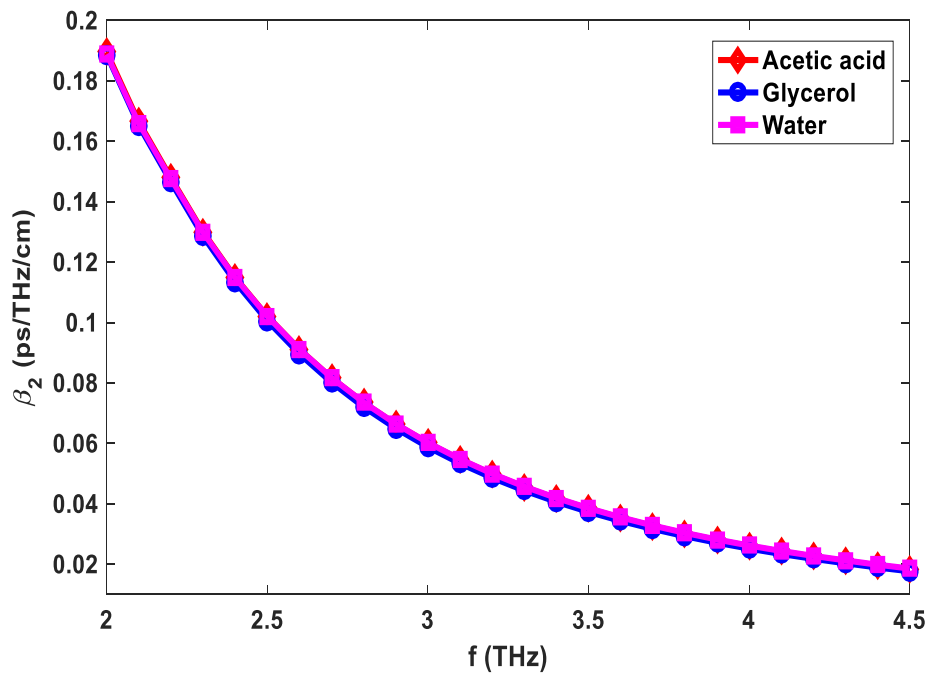
Fig. 5.8. Frequency vs. Dispersion for water, acetic acid and glycerol

In Fig. 5.9, A_{eff} decreases as frequency increases. As frequency increases; the signal becomes more and more confined within the core area. The more confined the core is, the smaller the effective area occupied by the signal. Therefore A_{eff} decreases as frequency increases.
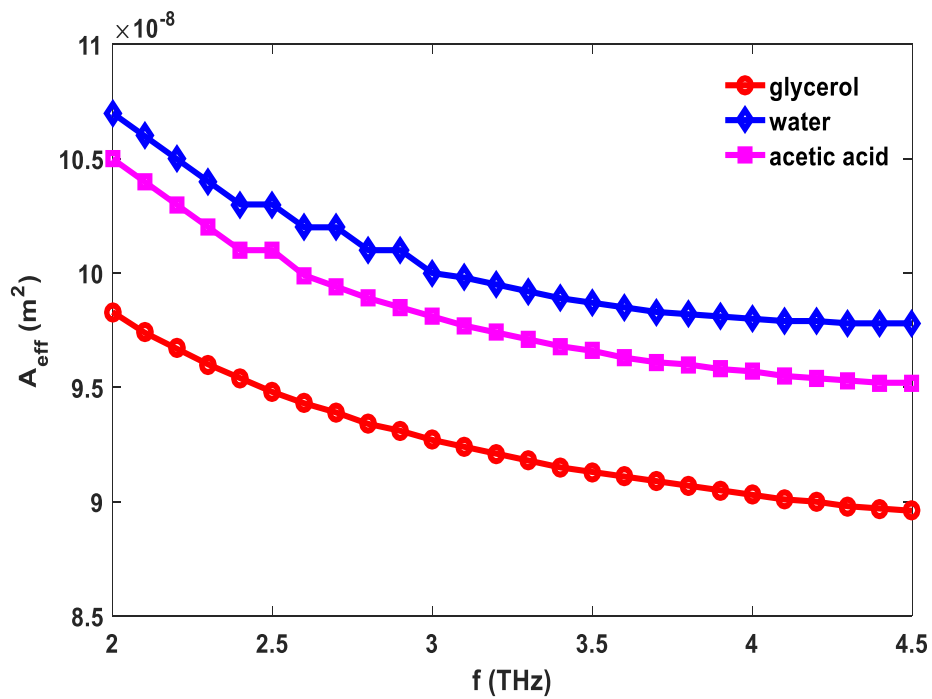
Fig. 5.9. Frequency vs. Effective Area (A_{eff}) for water, acetic acid and glycerol

Fig. 5.10 displays the relationship between numerical aperture (NA) and frequency. It can be seen that numerical aperture is inversely proportional to frequency provided all other parameters are kept constant. Moreover, for a constant operating frequency, numerical aperture is directly proportional to effective area. These two points implies that as the frequency increases, the numerical aperture is expected to decrease accordingly. Thus the curve decreases as the frequency is increased.
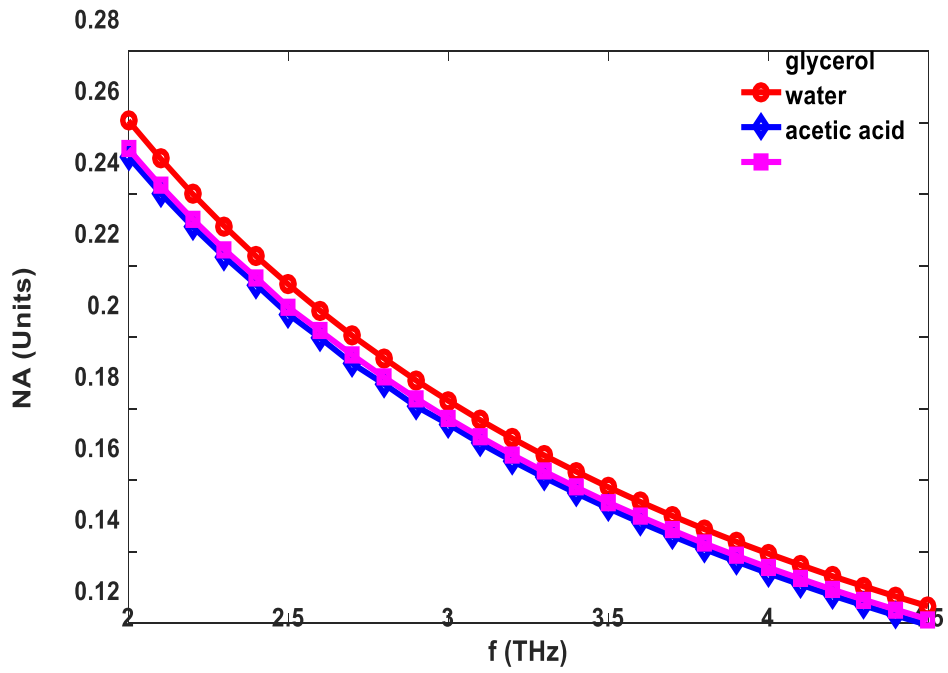
Fig. 5.10. Frequency vs. Numerical Aperture for water, acetic acid and glycerol

Table 5.1 Compares the sensitivity and EML of the proposed design to that of recent research works.

Table 5.1. Comparison of the sensitivity and EML of the proposed spider-web sensor design to those of previously reported sensors

PCF Designs	Sensitivity (%)	EML (cm^{-1})
[3]	-	0.052
[129]	-	±0.000416
[89]	49.17	-
[90]	53.35	-
[28]	55.56	-
[91]	57.18	-
[2]	61.45	-
[92]	62.19	-
[36]	69.09	-
[11]	85.7	-
[1]	96.8	0.0035
[45]	-	0.04
Spider Web	99.90	0.000113

In table 5.2 below, it can be seen that the proposed design has shown better results than recent reported works in the same field.

Table 5.2. Comparison of the performance characteristics between the proposed spider-web sensor design and previously reported sensors

PCF Designs	Confinement loss (dB/m)	Dispersion (ps/THz/cm)	Numerical Aperture (units)
[3]	-	2.2±0.25	-
[129]	1.2×10^{-9}	0.4±0.042	-
[89]	6.3×10^{-11}	-	-
[90]	3.7×10^{-11}	-	-
[28]	-	-	-
[91]	1.11×10^{-11}	-	-
[2]	1.41×10^{-10}	-	0.32
[92]	5.56×10^{-11}	-	-
[36]	4.99×10^{-9}	-	-
[11]	1.7×10^{-9}	0.47 ± 0.265	0.37
[1]	6.95×10^{-14}	-	-
[45]	-	0.98 ± 0.09	-
Spider Web	1.429×10^{-16}	0.017 ± 0.001	0.26

Table 5.3 summarizes the performance of the proposed sensor designs.

Table 5.3. Comparison between the proposed modified kagome vs. the proposed spider-web design

Parameter	Proposed Modified Kagome	Proposed Spider Web
Sensitivity	99.98	99.90
EML	0.000263	0.000113
Confinement loss	2.117×10^{-17}	1.429×10^{-16}
Dispersion	0.4	0.017 ± 0.001
Numerical aperture	0.33	0.26

5.4. Conclusion

A spider-web like hollowed core design was proposed for sensing applications. The proposed design displayed a sensitivity of 99.90%, a very low EML of 0.000113 cm^{-1} at 4.5 THz for glycerol. Important parameters like confinement loss, dispersion and numerical aperture were equally investigated and have shown to yield improved results compared to previously published research works. Finally, the proposed design is an ideal candidate as a sensor for a wide variety of sensing purposes.

CHAPTER 6

CONCLUSION AND FUTUR WORKS

6.1. Conclusion

Two octagonal hollowed cored designs with a modified Kagome- and Spider-web like claddings respectively were proposed and investigated varying several parameters to obtain the desired sensitivity for liquid sensing applications. More so, the maximum possible enhancement of the sensitivity, EML and design complexity of each of these designs were made a priority with respect to other parameters. Hence, even though the first proposed design (Modified Kagome) showed a better sensitivity and improved EML than previously reported works, compared to the second design (Spider web), the relatively lower sensitivity, higher EML and design complexity of the former makes the latter a better candidate for an accurate design implementation during fabrication. Appendix I and II compare the results obtained with of previously reported works. It is clearly seen that the proposed designs both showed far better results compared to previous works in same field. Finally, the proposed designs can be seen as very effective sensors that can be used ideally as chemical sensors bringing about an appreciable contribution into its respective field of research, that is, the oceanic field of PCFs based sensors.

Even though, the proposed designs display outstanding results, there still exist a number of limitations and challenges faced during this research process. The main limitations and challenges faced during this research includes:

> ➢ There is no allowance for real time monitoring of the sample analyte's interaction

- Speed, specificity and affinity of molecules' association and disassociation cannot be retrieve from simulation through the proposed method

- The limited and inadequate physical and online library resources with regards to COMSOL Multiphysics software

- High computational requirement of COMSOL Multiphysics software
- The high instability associated with the complex values of the effective mode indices due to operation at high frequencies i.e. above 1.5 THz

- Time consumption due to the cumbersome process of collecting, processing and retrieving data. This is because any potential error may result in a completely new simulation process and all previous efforts rendered vain.

6.2. Future Works

Future research areas may include sensitivity measurements based on Surface Plasmon Resonance (SPR). Surface Plasmon resonance refers to an optical phenomenon that allows the monitoring of changes in RI via quantum mechanical principles.

SFR is a label-free, proven biosensor technique used in studying interactions between all classes of biomolecules and biochemical mechanisms in real time. SFR sensors are the current trend in recent sensing and similar technologies, and are becoming even more important across a number of fields. SFR has innumerable advantages as it is possible to know how fast molecules associate and disassociate, how strong they interact, how specific is the interaction and what is the interaction of the interactants.

Basically, four (04) main steps are required in a classic SFR experiment [117], namely;

> A target is captured or immobilized onto a surface, referred to as sensor chip

> Analytes are been flown unto the sensor chip using a pump

> Changes occurring on the surface of the sensor chip is are then captured using an optical measurement system

> A software then plots time-dependent responses in the form of a graph known as a sensor gram

The main advantages of SFR sensors [118] are;

> Label-free detection: Since differences in RI are detected using SFR, there is no need for any label detection.

> Small samples sizes: A minimal amount of sample is required to run an experiment using SFR. Hence, scientists and healthcare professionals may use less number of expensive materials saving money and making SFR more affordable and accessible.

> Reusable sensor chips: Sensor chips influence directly is a vital component and influence directly data quality, thus, its ability to be reused is highly cost effective.

> Ability to replicate measurement: Replicate injections of the same concentration throughout a run can be done repeatedly. This further increases result accuracy.

- ➢ Real-time monitoring: SFR technology provides a relatively affordable and simple way of observing different biomolecules interaction in real time.

- ➢ Ability to handle complex samples: SFR has been used for testing samples in a variety of complicated matrices, including situations where only crude samples are available for testing.

Applications areas of SFR are medical diagnosis, colorimetric sensor, organic chemical sensing, telemedicine, glucose monitor, disease detection, bio imaging, environmental monitoring and chemical sensing [119].

REFERENCES

[1] Md. Saiful Islam et al., "Terahertz Sensing in a Hollow Core Photonic Crystal Fiber," IEEE Sensors Journal, vol.18, no.10, pp. 1-8, May 15, 2018.

[2] S. Chowdhury et al., "Design of Highly Sensible porous Shaped Photonic Crystal Fiber with Strong Confinement Field for Optical Sensing," Optik-International Journal for Light and Electron Optics, pp. 541-549, 2017.

[3] Md. R. Hasan et al., "Dual-hole unit based kagome lattice microstructure fiber for low-loss and highly birefringent terahertz guidance," Optical Engineering, vol. 56, no. 4, pp. 043108, 2017.

[4] P. H. Bolívar et al., "Label-free THz sensing of genetic sequences: towards THz biochips," Philos. Trans. R. Soc., A: Math. Phys. Eng. Sci., vol. 362, no.1815, pp. 323–335, 2004.

[5] M. M. Awad and R. A. Cheville, "Transmission terahertz waveguide based imaging below the diffraction limit," Applied Physic Letters, vol. 86, no. 20, pp. 221107, 2005.

[6] M. Nagel et al., "Integrated THz technology for label-free genetic diagnostics," Appl. Phys. Lett., vol. 80, no. 1, pp. 154–156, 2002.

[7] C. J. Strachan et al., "Using terahertz pulsed spectroscopy to quantify pharmaceutical polymorphism and crystallinity," J. Pharm. Sci., vol. 94, no. 4, pp. 837–846, 2005.

[8] V. P. Wallace et al., "Terahertz pulsed imaging of basal cell carcinoma ex vivo and in vivo," Br. J. Dermatol., vol. 151, no. 2, pp. 424–432, 2004.

[9] Y. C. Shen et al., "Detection and identification of explosives using terahertz pulsed spectroscopic imaging," Applied Physics Letters, vol. 86, no. 24, pp. 241116, 2005.

[10] N. Laman et al., "7 GHz resolution waveguide THz spectroscopy of explosives related solids showing new features," Opt. Express, vol. 16, no. 6, pp. 4094–4105, 2008.

[11] Md. Saiful Islam et al., "A Novel Approach for Spectroscopic Chemical Identification Using Photonic Crystal Fiber in the Terahertz Regime," IEEE Sensors Journal, vol.18, no. 2, pp. 1-8, Jan. 15, 2018.

[12] Yang X. C. et al., "Temperature Sensor Based on Photonic Crystal Fibre Filled with Liquid and Silver Nanowires," IEEE Photonics Journal, vol. 8, no. 3, June, 2016.

[13] Ademgil H. and Haxha S., "PCF based Sensor with high Sensitivity, high birefringence and Low Confnement Losses for Liquid Analyte Sensing Applications," Sensors, vol. 15, no. 12, pp. 31833-31842, 2015.

[14] Khan M. R. R. and Kang S. W., "Highly Sensitive Temperature Sensors Based on Fibre-Optic PWM and Capacitance Variation Using Thermochromic Sensing Membrane," Sensors, vol. 16, no. 7, pp. 1064, 2016. MDPI article

[15] Zan X. et al., "The research on temperature sensing properties of photonic crystal fibre based on Liquid crystal filling," MATEC web of Conferences, vol. 61, pp. 06009, 2016.

[16] Liu H. et al., "Curvature and Temperature Measurement based on a Few-Mode PCF formed M-Z-I and an Embedded FBG," Sensors, vol. 17, no. 8, pp. 1725, 2017. MDPI article.

[17] Dash J. N. and Jha R., "PCF Modal interferometer based on macrobending for refractive index sensing," IEEE Sensors Journal, vol. 15, no.9, pp. 5291-5295, 2015.

[18] Sun B. et al., "Asymmetrical in-fibre Mach-Zehnder interferometer for curvature measurement," Optical Society of America, vol. 23, no. 11, pp. 14596-14602, 2015.

[19] E. I. Pacheco-Chac_on et al., "Temperature sensing setup based on an aluminum coated Mach-Zehnder Interferometer," Proc. of SPIE, vol. 10231, 2017.

[20] Liu C. et al., "Design and theoretical analysis of a photonic crystal fibre based on surface Plasmon resonance sensing," Journal of Nanophotonics, vol. 9, no. 1, pp. 093050, 2015.

[21] K. Ahmed et al., "Optimization and enhancement of liquid analyte sensing performance based on square-cored octagonal photonic crystal fiber," Optik – Int. J. Light Electron Opt., vol. 131, pp. 687–696, 2017.

[22] B. K. Paul et al., "Folded cladding porous shaped photonic crystal fiber with high sensitivity in optical sensing applications: design and analysis," Sens. Bio-Sens. Res., Vol. 12, pp. 36–42, 2017.

[23] N. A. Mortensen et al., "Photonic crystal fiber with a hybrid honeycomb cladding," Opt. Express, vol. 12, no. 3, pp. 468, 2000.

[24] A. Agrawal et al., "Soft glass equiangular spiral photonic crystal fiber for supercontinuum generation," IEEE Photon. Technol. Lett., vol. 21, no. 22, pp. 1722–1724, 2009.

[25] H. Ademgil, "Highly sensitive octagonal photonic crystal fiber based sensor," Optik International Journal for Light and Electron Optics, vol. 125, no. 20, pp. 6274–6278, 2014.

[26] S. M. A. Razzak et al., "Design of a decagonal photonic crystal fiber for ultra-flattened chromatic dispersion," IEICE Transactions on Electronics, vol. 90, no. 11, pp. 2141–2145, 2007.

[27] S. Asaduzzaman et al., "Hybrid photonic crystal fiber in chemical sensing," SpringerPlus, vol. 5, no. 1, pp. 1–11, 2016.

[28] M. S. Islam et al., "Liquid-infiltrated photonic crystal fiber for sensing purpose: Design and analysis," Alexandrai Engineering Journal, pp. 1-8, 2017.

[29] Y.-H. Lin et al., "Using graphene nano-particle embedded in photonic crystal fiber for evanescent wave mode-locking of fiber laser," Opt. Express, vol. 21, no. 14, pp. 16763, 2013.

[30] V. V. R. K. Kumar et al., "Tellurite photonic crystal fiber," Opt. Express, vol. 11, no. 20, pp. 2641, 2003.

[31] S. Atakaramians et al., "Porous fibers: a novel approach to low loss THz waveguides," Opt. Express, vol. 16, no. 12, pp. 8845–8854, 2008.

[32] M. Goto et al., "Teflon photonic crystal fiber as terahertz waveguide," Jpn. J. Appl. Phys., vol. 43, no. 2B, pp. L317–L319, 2004.

[33] K. Nielsen et al., "Bendable, low-loss Topas fibers for the terahertz frequency range," Opt. Express, vol. 17, no. 10, pp. 8592–8601, 2009.

[34] C. Markos, I. Kubat and O. Bang, "Hybrid polymer photonic crystal fiber with integrated chalcogenide glass nanofilms", Sci. Rep., vol. 4, pp. 6057, August 2014.

[35] J.N. Dash and R. Jha, "Graphene-based birefringent photonic crystal fiber sensor using surface plasmon resonance," IEEE Photonics Technol. Lett., vol. 26, no. 11, pp. 1092-1095, June 2014.

[36] Paul, M. Islam, K. Ahmed and S. Asaduzzaman, "Alcohol sensing over O+E+S+C+L+U transmission band based on porous core octogonal photonic crystal fiber," Photonic Sensors, pp. 1-8, 2017.

[37] J. D. Shephard et al., "Single-mode mid-IR guidance in a hollow-core photonic crystal fiber," Opt. Exp., vol. 13, no. 8, pp. 7139–7144, 2005.

[38] P. J. Roberts et al., "Ultimate low loss of hollow-core photonic crystal fibres," Opt. Exp., vol. 13, no. 1, pp. 236–244, 2005.

[39] B. A. Riyadh S. M. et al. "Photonic Crystal Fibers for Sensing Applications",J Biosens Bioelectron, vol. 9, no. 1, pp. 1-7, 2018.

[40] M. Mattia et al., "Hollow core fibers for high power laser applications" Optics Express, vol. 24, no. 7, pp. 7103-7119, 2016.

[41] S. Asaduzzaman, M. F. H. Arif, K. Ahmed and P. Dhar, "Highly sensitive simple structure circular photonic crystal fiber based chemical sensor," IEEE Int. WIE Conf. Electr. Comput. Eng., pp. 1-5, 2015.

[42] Y. Huang, Y. Xu and A. Yariv, "Fabrication of functional micro structured optical fibers through a selective-filling technique," Appl. Phys. Lett., vol. 85, no. 22, pp. 5182, 2004.

[43] "Fabrications of photonic crystal fibers", Photonic crystal fibre science, http://www.mpl.mpg.de/en/russell/research/topics/fabrication.html.

[44] H. Ebendorff-Heidepriem, J. Schuppich, A. Dowler, L. Lima-Marques and T. Monro, "3Dprinted extrusion dies: a versatile approach to optical material processing," Opt. Mater. Exp., vol. 4, no. 8, pp. 1494–1504, 2014.

[45] J. Sultana et al., "Design and analysis of a Zeonex based diamond-shaped core kagome lattice photonic crystal fiber for T-ray wave transmission", Optical Fiber Technology, vol. 47, pp. 55–60, 2019.

[46] J. Chamberlain, "where optics meets electronics: recent progress in decreasing the terahertz gap," Philos. Trans. R. Soc. A., vol. 362, pp. 199–213, 2004.

[47] K. M. Kiang et al., "Extruded singlemode non-silica glass holey optical fibres," Electron. Lett., vol. 38, no. 12, pp. 546–547, 2002.

[48] Hanaor, D. A. H. et al., "Single and Mixed Phase TiO2 Powders Prepared by Excess Hydrolysis of Titanium Alkoxide", Advances in Applied Ceramics, vol. 111, no. 3, pp. 149–158, 2012. arXiv:1410.8255. doi:10.1179/1743676111Y.0000000059.

[49] Brinker, C. J. et al., "Sol-Gel Science: The Physics and Chemistry of Sol-Gel Processing", Academic Press, 1990. ISBN 978-0-12-134970-7.

[50] Hench, L. L. et al. "The Sol-Gel Process". Chemical Reviews, 1990. 90: 33–72. doi:10.1021/cr00099a003.

[51] Klein L., "Sol-Gel Optics: Processing and Applications" Springer Verlag, 1994. ISBN 978-0 7923-9424-2.

[52] Kumar A. et al., "Sol-Gel Derived Nanomaterials and Its Applications: A Review", Research Journal of Chemical Sciences, Vol. 5, no. 12, pp. 98-105, December 2015.

[53] Verwey E. J. W. et al., "Colloid Science", Elsevier, Amsterdam, The Netherlands, vol. 1, 1948.

[54] Hench L. L. and West J. K., Chem. Rev., vol. 90, pp. 33-72, 1990

[55] Wohlers, Terry, Wohlers report, Wohlers Associates, Inc, 2016.

[56] "3D Printing: Challenges and Opportunities for International Relations". Council on Foreign Relations, October 23, 2013. Archived from the original on 2013-10-28. Retrieved 2013-10-30.

[57] Griffiths L. "How desktop 3D printers became an essential industry tool", TCT Magazine, 2018. Retrieved 2018-11-28.

[58] "Royal Netherlands Air Force recruits Ultimate 3D printers for maintenance and repair operations", 3D Printing Industry, 2019. Retrieved 2019-01-11.

[59] "F-35 stealth fighter gets boost from 3D printing", 3D Printing Industry, 2018. Retrieved 2019-01-11.

[60] "Despite Market Woes, 3D Printing Has a Future Thanks to Higher Education - Bold", 2 December 2015.

[61] "Stratasys Ltd. Short Interest Update", Americantradejournal.com.

[62] H. Stephen et al., "Modular 3D Printed Compressed Air Driven Continuous-Flow Systems for Chemical Synthesis", 2019. doi:10.26434/chemrxiv.7781033.v1.

[63] "UMass Amherst Library Opens 3-D Printing Innovation Center"

[64] https://markforged.com/learn/3d-printer-types-technologies/

[65] Bickel B. et al., "State of the Art on Stylized Fabrication" (PDF). Computer Graphics Forum, vol. 37, no. 6, pp. 325–342, 2018. doi:10.1111/cgf.13327

[66] https://markforged.com/learn/how-do-3d-printers-work/

[67] https://markforged.com/learn/what-is-3d-printing/

[68] J. L. Wasserman; et al., "Fabrication of One-Dimensional Programmable-Height Nanostructures via Dynamic Stencil Deposition", Review of Scientific Instruments, vol. 79, no. 7, pp. 073909–073909–4, 2008. arXiv:0802.1848. Bibcode:2008RScI...79g3909W. doi:10.1063/1.2960573. PMID 18681718.

[69] Patel P. "Micro 3-D Printer Creates Tiny Structures in Seconds", MIT Technology Review, March 2013.

[70] https://www.laserfocusworld.com/lasers-sources/article/16559241/midir-erbiumdoped-zblan-fiber-laser-is-widely-tunable

[71] https://www.sciencedaily.com/releases/2018/01/180117102644.htm

[72] Yong-Lai Zhang et al., "Designable 3D nanofabrication by femtosecond laser direct writing", NanoToday, vol. 5, pg. 435-448, 2010.

[73] "Additive manufacturing — General Principles — Overview of process categories and feedstock", ISO/ASTM International Standard, pp. 17296-2:2015(E), 2015.

[74] O'Neal and Bridget Butler, "UCL School of Pharmacy: 3D Prints Affordable Continuous Flow Systems", *3DPrint.com | The Voice of 3D Printing / Additive Manufacturing, 2019. Retrieved 2019-03-12.*

[75] J. Han, S. Li, and T. Zhang, "Design on a novel hybrid-core photonic crystal fiber with large birefringence and high nonlinearity," Opt. Quantum Electron., vol. 48, pp. 1–11, 2016.

[76] S. Roy, S. F. Kayser, and T. Azmaeen, "Design and optimization of a single mode octagonal photonic crystal fiber for high negative dispersion and high nonlinearity," Int. Conf. Inf. Electron. Vis., pp. 614–619, 2016.

[77] H. Valtna-Lukner, J. Repan, S.M. Valdma, and P. Piksarv, "Endlessly single-mode photonic crystal fiber as a high resolution probe," Appl. Opt., vol. 55, pp. 9407–9411, 2016.

[78] "Attenuation by Atmospheric Gases," International Telecommunication Union ITU-R Recommendation, P. 676–10, 2013.

[79] T. Nagatsuma, G. Ducournau, and C.C. Renaud, "Advances in terahertz communications accelerated by photonics," Nat. Photon., vol. 10, pp. 371–379, 2016.

[80] Md. S. Islam, J. Sultana, A. Dinovitser, Brian W.H. Ng, and D. Abbott, "A novel zeonex based oligoporous-core photonic crystal fiber for polarization preserving terahertz applications," Opt. Commun., vol. 413, no. 15, pp. 242–248, 2018.

[81] K. Ahmed, S. Chowdhury, B. K. Paul, M. S. Islam, S. Sen, M. I. Islam, and S. Asaduzzaman, "Ultrahigh birefringence, ultralow material loss porous core single-mode fiber for terahertz wave guidance," Appl. Opt., vol. 56, pp. 3477–3483, 2017.

[82] P. Yeh, A. Yariv, and E. Marom, "Theory of Bragg fiber," Journal of the Optical Society of America, vol. 68, no. 9, pp. 1196–1201, 1978.

[83] X. Jiaqiang, C. Yuping, C. Daoyong, and S. Jianian, "Hydrothermal synthesis and gas sensing characters of ZnO nanorods," Sens. Actuators B, Chem., vol. 113, no. 1, pp. 526–531, 2006.

[84 P. U. Jepsen, U. Møller, and H. Merbold, "Investigation of aqueous alcohol and sugar solutions with reflection terahertz time-domain spectroscopy," Opt. Exp., vol. 15, no. 22, pp. 14717–14737, 2007.

[85] P. U. Jepsen, J. K. Jensen, and U. Møller, "Characterization of aqueous alcohol solutions in bottles with THz reflection spectroscopy," Opt. Exp., vol. 16, no. 13, pp. 9318–9331, 2008.

[86] E. Arik, C. Koral, H. Altan, and O. Esenturk, "A new method for alcohol content determination of fuel oils by terahertz spectroscopy," in Proc. 38th Int. Conf. Infr., Millim., Terahertz Waves (IRMMW-THz), Mainz, Germany, vol. 1, September, 2013.

[87] K. Ahmed and M. Morshed, "Design and numerical analysis of microstructured-core octagonal photonic crystal fiber for sensing applications," Sensing and Bio-Sensing Research, vol. 7, pp. 1–6, 2016.

[88] S. Asaduzzaman, K. Ahmed, T. Bhuiyan, and T. Farah, "Hybrid photonic crystal fiber in chemical sensing," SpringerPlus, vol. 5, no. 1, pp. 1–11, 2016.

[89] S. Asaduzzaman, K. Ahmed, T. Bhuiyan, and T. Farah, "Hybrid photonic crystal fiber in chemical sensing," SpringerPlus, vol. 15, no. 1, p. 748, 2016.

[90] F. H. Arif and J. H. Biddut, "A new structure of photonic crystal fiber with high sensitivity, high nonlinearity, high birefringence and low confinement loss for liquid analyte sensing applications," Sens. Bio-Sens. Res., vol. 12, pp. 8–14, Feb. 2017.

[91] S. Sen, S. Chowdhury, and K. Ahmed et al., "Design of A Porous Cored Hexagonal Photonic Crystal Fiber Based Optical Sensor with High Relative

Sensitivity for Lower Operating Wavelength," Photonic Sensors, vol. 7, no. 1, pp. 55-65, 2017.

[92] Kawsar Ahmed et al., "Design and numerical analysis: Effect of core and cladding area on hybrid hexagonal microstructure optical fiber in environment pollution sensing applications," Karbala International Journal of Modern Science, pp. 1-10, March 2017.

[93] S.-Jin Im, A. Husakou, and J. Herrmann, "Guiding properties and dispersion control of kagome lattice hollow-core photonic crystal fibers," Opt. Exp., vol. 17, pp. 13050–13058, 2017.

[94] J. V. Neuman, and E. Wigner, "On curious discrete eigenvalues," Phys. Z., vol. 30, pp. 465–467, 1975.

[95] M. Morshed, S. Asaduzzaman, M. F. H. Arif, and K. Ahmed, "Proposal of simple gas sensor based on micro structure optical fiber," International Conference on Electrical Engineering and Information Communication Technology (ICEEICT), 2015.

[96] G.K.M. Hasanuzzaman, M.S. Habib, S.M.A. Razzak, M.A. Hossain, and Y. Namihira, "Low loss single mode porous-core kagome photonic crystal fiber for THz wave guidance," J. Light-wave Technol., vol. 33, pp. 15400618, 2015.

[97] S. Asaduzzaman and K. Ahmed, "Proposal of a gas sensor with high sensitivity, birefringence and nonlinearity for air pollution monitoring," Sensing and Bio-Sensing Research, vol. 10, no. 1, pp. 20–26, 2016.

[98] J. D. Shephard et al., "Single-mode mid-IR guidance in a hollow-core photonic crystal fiber," Opt. Exp., vol. 13, no. 8, pp. 7139–7144, 2005.

[99] P. J. Roberts et al., "Ultimate low loss of hollow-core photonic crystal fibres," Opt. Exp., vol. 13, no. 1, pp. 236–244, 2005.

[100] M. R. Hasan, M. S. Anwar, Md. I. Hasan, and S. M. A. Razzak, "Polarization maintaining low-loss slotted core kagome lattice THz fiber," IEEE Photon. Technol. Lett., vol. 28, pp. 1751–1754, 2016.

[101] J. Anthony, R. Leonhardt, A. Argyros, and M. C. J. Large, "Characterization of a microstructured Zeonex terahertz fiber," J. Opt. Soc. Amer. B, Opt. Phys., vol. 28, no. 5, pp. 1013–1018, May 2011.

[102] ZEONEX Grade Review for Optical Applications. Accessed: Mar. 29, 2018. [Online]. Available: https://www.zeonex.com/optics. aspx.html#products

[103] G. Woyessa, A. Fasano, C. Markos, A. Stefani, H. K. Rasmussen, and O. Bang, "Zeonex microstructured polymer optical fiber: Fabrication friendly fibers for high temperature and humidity insensitive Bragg grating sensing," Opt. Mater. Exp., vol. 7, no. 1, pp. 286–295, 2017.

[104] H. Han, H. Park, M. Cho, and J. Kim, "Terahertz pulse propagation in a plastic photonic crystal fiber," Appl. Phys. Lett., vol. 80, no. 15, p. 2634, 2002.

[105] M. S. Islam et al., "Extremely low material loss and dispersion flattened TOPAS based circular porous fiber for long distance terahertz wave transmission," Opt. Fiber Technol., vol. 34, pp. 6–11, March, 2016.

[106] *G. P. Nikishkov, "Introduction to The Finite Element Method", 2004 Lecture Notes. University of Aizu, Aizu-Wakamatsu 965-8580, Japan*

[107] https://www.machine dsign.com/fea-analysis-and-simulation

[108] M.F.H. Arif, K. Ahmed, S. Asaduzzaman, and M.A.K. Azad, "Design and optimization of photonic crystal fiber for liquid sensing applications," Photonic Sensors, vol. 6, no. 3, pp. 279–288, 2016.

[109] J. Liang, L. Ren, N. Chen, and C. Zhou, "Broadband, low-loss, dispersion flattened porous-core photonic bandgap fiber for terahertz (THz)- wave propagation," Opt. Commun., vol. 295, pp. 257–261, May 2013.

[110] Sohel Rana et al., "Low Loss and Low Dispersion Fiber for Transmission Applications in the Terahertz Regime", IEEE Photonics Technology Letters, vol. 29, no. 10, May 15, 2017.

[111] M. R. Hasan, S. Akter, T. Khatun, A. A. Rifat, and M. S. Anower, "Dual-hole unit-based kagome lattice microstructure fiber for low-loss and highly birefringent terahertz guidance," Opt. Eng., Vol. 56, pp. 043108, 2017.

[112] M. F. H. Arif, and M .J. H. Biddut, "Enhancement of relative sensitivity of photonic crystal fiber with high birefringence and low confinement loss," Optik Int. J. Light Electron Opt., vol. 131, pp. 697-704, February, 2017.

[113] https://www.msdsonline.com/2014/11/19/acetic-acid-hazards-safety information/

[114] https://www.webmd.com/vitamins/ai/ingredientmono-4/glycerol

[115] https://www.drugs.com/sfx/glycerol-side-effects.html

[116] https://www.toppr.com/guides/biology/natural-resources/water-and-water-pollution/

[117] https://www.reichertspr.com/about/what-is-suface-plasmon-resonance-spr/

[118] https://www.reichertspr.com/blog/2015/10/28/the-advantages-of-spr-technology/

[119] https://www.researchgate.net/figure/Applications-of-surface-plasmon-resonance-sensors_fig1_325845992

[120] https://www.comsol.com/

[121] https://en.wikipedia.org/wiki/COMSOL_Multiphysics/

[122] https://soft-hummingbird.com/

[123] https://www.g2crowd.com/products/comsol-multiphysics-formerly-femlab/reviews

[124] K. Ahmed and M. Morshed, "Design and numerical analysis of microstructured-core octagonal photonic crystal fiber for sensing applications," Sensing and Bio-Sensing Research, vol. 7, pp. 1–6, 2016.

[125] R. Islam, Md. S. Habib, G. K. M. Hasanuzzaman, S. Rana, Md. A. Sadath, and C. Markos, "A novel low-loss diamond-core porous fiber for polarization maintaining terahertz transmission," IEEE Photon. Technol. Lett., vol. 28, pp. 1737–1740, 2016.

[126] S. Asaduzzaman, K. Ahmed, and B.K. Paul, "Slotted-core photonic crystal fiber in gas sensing application, in: Proc. of SPIE, vol. 10025, pp. 1-9, 2016.

[127] M.F.H. Arif, S. Asaduzzaman, M.J.H. Biddut, and K. Ahmed, "Design and optimization of highly sensitive photonic crystal fiber with low confinement loss for ethanol detection," Int. J. Technol., vol. 6, pp. 1068-1076, 2016.

[128] X. Zhang, M. He, M. Chang et al., "Dual-cladding high-birefringence and high-nonlinearity photonic crystal fiber with As_2S_3 core," Optics Communication, vol. 410, pp. 396-402, 2018.

[129] S. Ali, N. Ahmed, S. Alwee et al., "Effects of Triangular Core Rotation of a Hybrid Porous Core Terahertz Waveguide," INTL Journal of Electronics and Telecommunications, vol. 63, no. 1, pp. 25-31, 2017.